Advances in Chemical Physics **135** (2007) 83-133

# Time asymmetry in nonequilibrium statistical mechanics

Pierre Gaspard
*Center for Nonlinear Phenomena and Complex Systems,*
*Université Libre de Bruxelles, Code Postal 231, Campus Plaine, B-1050 Brussels, Belgium*

An overview is given on the recent understanding of time asymmetry in nonequilibrium statistical mechanics. This time asymmetry finds its origin in the spontaneous breaking of the time-reversal symmetry at the statistical level of description. The relaxation toward the equilibrium state can be described in terms of eigenmodes of fundamental Liouville's equation of statistical mechanics. These eigenmodes are associated with Pollicott-Ruelle resonances and correspond to exponential damping. These eigenmodes can be explicitly constructed in dynamical systems sustaining deterministic diffusion, which shows their singular character. The entropy production expected from nonequilibrium thermodynamics can be derived *ab initio* thanks to this construction. In the escape-rate theory, the transport coefficients can be related to the leading Pollicott-Ruelle resonance of open systems and to the characteristic quantities of the microscopic dynamics. In nonequilibrium steady states, the entropy production is shown to result from a time asymmetry in the dynamical randomness of the nonequilibrium fluctuations. Furthermore, the generalizations of Onsager reciprocity relations to nonlinear response can be deduced from the fluctuation theorem for the currents. Furthermore, the principle of temporal ordering in nonequilibrium steady states is formulated and its perspectives for the generation of biological information are discussed.

## I. INTRODUCTION

Natural phenomena are striking us every day by the time asymmetry of their evolution. Various examples of this time asymmetry exist in physics, chemistry, biology, and the other natural sciences. This asymmetry manifests itself in the dissipation of energy due to friction, viscosity, heat conductivity, or electric resistivity, as well as in diffusion and chemical reactions. The second law of thermodynamics has provided a formulation of their time asymmetry in terms of the increase of the entropy. The aforementioned irreversible processes are fundamental for biological systems which are maintained out of equilibrium by their metabolic activity.

These phenomena are described by macroscopic equations that are not time-reversal symmetric in spite of the fact that the motion of the particles composing matter is ruled by the time-reversal symmetric equations of Newton or Schrödinger. This apparent dichotomy has always been very puzzling. Recently, a new insight into this problem has come from progress in dynamical systems theory. The purpose of dynamical systems theory is to analyze the trajectories of dynamical systems and to describe their statistical properties in terms of invariant probability measures. This theory has been developed to understand, in particular, how deterministic systems ruled by ordinary differential equations such as Newton's equation can generate random time evolutions, the so-called chaotic behaviors. New concepts such as the Lyapunov exponents, the Kolmogorov-Sinai entropy per unit time, the Pollicott-Ruelle resonances, and others have been discovered which are important additions to ergodic theory [1]. These new concepts have been used to revisit the statistical mechanics of irreversible processes, leading to advances going much beyond the early developments of ergodic theory. Thanks to these advances, it is nowadays possible to understand in detail how a system ruled by time-reversal symmetric Newton equations can generate a relaxation toward the state of thermodynamic equilibrium and thus to explain how the time asymmetry can appear in the statistical description. Furthermore, new relationships have been derived about the properties of the fluctuations in nonequilibrium systems, in particular, for the dissipated work [2]. These new relationships are based on the description of nonequilibrium systems in terms of paths or histories, description to which dynamical systems theory has greatly contributed.

Very recently, a new concept of time-reversed entropy per unit time was introduced as the complement of the Kolmogorov-Sinai entropy per unit time in order to make the connection with nonequilibrium thermodynamics and its entropy production [3]. This connection shows that the origin of entropy production can be attributed to a time asymmetry in the dynamical randomness of nonequilibrium steady states. Dynamical randomness is the property that the paths or histories of a fluctuating system do not repeat themselves and present random time evolutions. Examples are stochastic processes such as coin tossing or dice games of chance. The paths or histories of these processes can be depicted in space-time plots, representing the time evolution of their state. The disorder of the state of the system at a given time is characterized by the thermodynamic entropy or the entropy per unit volume. In contrast, the dynamical randomness can be characterized by the concept of entropy per unit time, which is a measure of disorder along the time axis instead of the space axis. Under nonequilibrium conditions, a time asymmetry appears in the dynamical

randomness measured either forward or backward in time with the Kolmogorov-Sinai entropy per unit time or the newly introduced time-reversed entropy per unit time. The difference between both quantities is precisely the entropy production of nonequilibrium thermodynamics [3]. This new result provides an interpretation of the second law of thermodynamics in terms of temporal ordering out of equilibrium, which has far reaching consequences for biology as will be explained below.

These new methods of nonequilibrium statistical mechanics can be applied to understand the fluctuating properties of out-of-equilibrium nanosystems. Today, nanosystems are studied not only for their structure but also for their functional properties. These properties are concerned by the time evolution of the nanosystems and are studied in nonequilibrium statistical mechanics. These properties range from the electronic and mechanical properties of single molecules to the kinetics of molecular motors. Because of their small size, nanosystems and their properties such as the currents are affected by the fluctuations which can be described by the new methods.

The plan of the paper is the following. Section II gives a summary of the phenomenology of irreversible processes and set up the stage for the results of nonequilibrium statistical mechanics to follow. In Sec. III, it is explained that time asymmetry is compatible with microreversibility. In Sec. IV, the concept of Pollicott-Ruelle resonance is presented and shown to break the time-reversal symmetry in the statistical description of the time evolution of nonequilibrium relaxation toward the state of thermodynamic equilibrium. This concept is applied in Sec. V to the construction of the hydrodynamic modes of diffusion at the microscopic level of description in the phase space of Newton's equations. This framework allows us to derive *ab initio* entropy production as shown in Sec. VI. In Sec. VII, the concept of Pollicott-Ruelle resonance is also used to obtain the different transport coefficients, as well as the rates of various kinetic processes in the framework of the escape-rate theory. The time asymmetry in the dynamical randomness of nonequilibrium systems and the fluctuation theorem for the currents are presented in Sec. VIII. Conclusions and perspectives in biology are discussed in Sec. IX.

## II. HYDRODYNAMICS AND NONEQUILIBRIUM THERMODYNAMICS

### A. Hydrodynamics

At the macroscopic level, matter is described in terms of fields such as the velocity, the mass density, the temperature, and the chemical concentrations of the different molecular species composing the system. These fields evolve in time according to partial differential equations of hydrodynamics and chemical kinetics.

A fluid composed of a single species is described by five fields: the three components of the velocity, the mass density, and the temperature. This is a drastic reduction of the full description in terms of all the degrees of freedom of the particles. This reduction is possible by assuming the local thermodynamic equilibrium according to which the particles of each fluid element have a Maxwell-Boltzmann velocity distribution with local temperature, velocity, and density. This local equilibrium is reached on time scales longer than the intercollisional time. On shorter time scales, the degrees of freedom other than the five fields manifest themselves and the reduction is no longer possible.

On the long time scales of hydrodynamics, the time evolution of the fluid is governed by the five laws of conservation of mass, momenta, and energy:

$$\partial_t \, \rho = -\boldsymbol{\nabla} \cdot (\rho \boldsymbol{v}) \tag{1}$$

$$\partial_t \, \rho \boldsymbol{v} = -\boldsymbol{\nabla} \cdot (\rho \boldsymbol{v}\boldsymbol{v} + \boldsymbol{P}) \tag{2}$$

$$\partial_t \, \rho e = -\boldsymbol{\nabla} \cdot (\rho e \boldsymbol{v} + \boldsymbol{J}_q) - \boldsymbol{P} : \boldsymbol{\nabla} \boldsymbol{v} \tag{3}$$

where $\rho$ is the mass density, $\boldsymbol{v}$ the fluid velocity, and $e$ is the specific internal energy or internal energy per unit mass [4]. The pressure tensor $\boldsymbol{P}$ decomposes into the hydrostatic pressure $P$ and a further contribution due to the viscosities:

$$P_{ij} = P \, \delta_{ij} + \Pi_{ij} \tag{4}$$

with the components $i, j = x, y, z$. Both the viscous pressure tensor $\boldsymbol{\Pi}$ and the heat current density $\boldsymbol{J}_q$ are expressed in terms of the gradients of the velocity and the temperature by the phenomenological relations

$$\Pi_{ij} = -\eta \left( \nabla_i v_j + \nabla_j v_i - \frac{2}{3} \boldsymbol{\nabla} \cdot \boldsymbol{v} \, \delta_{ij} \right) - \zeta \, \boldsymbol{\nabla} \cdot \boldsymbol{v} \, \delta_{ij} \tag{5}$$

$$J_{q,i} = -\kappa \, \nabla_i T \tag{6}$$

where $\eta$ is the shear viscosity, $\zeta$ the bulk velocity, and $\kappa$ the heat conductivity.

TABLE I: The five hydrodynamic modes of a one-component fluid. $k$ is the wavenumber, $U_s$ the sound velocity, $\Gamma$ the damping coefficient (11), $\eta$ the shear viscosity, $\rho_0$ the uniform mass density, $\kappa$ the heat conductivity, and $c_P$ the specific heat capacity at constant pressure [4].

| mode | dispersion relation | multiplicity |
|---|---|---|
| longitudinal sound modes | $s \simeq \pm i\, U_s\, k - \Gamma k^2$ | 2 |
| shear modes | $s \simeq -\frac{\eta}{\rho_0} k^2$ | 2 |
| thermal mode | $s \simeq -\frac{\kappa}{\rho_0 c_P} k^2$ | 1 |

The hydrodynamic equations rule in particular the relaxation of the fluid toward its state of global thermodynamic equilibrium, in which the velocity vanishes while the hydrostatic pressure and the temperature become uniform. The approach to the global thermodynamic equilibrium can be described by linearizing the hydrodynamic equation around the equilibrium state. These linearized equations can be solved by using the principle of linear superposition. Accordingly, the general solution is the linear combination of special solutions which are periodic in space with a wavenumber $\boldsymbol{k}$ giving the direction of the spatial modulations and their wavelength $\lambda = 2\pi/\|\boldsymbol{k}\|$:

$$\rho(\boldsymbol{r},t) = \tilde{\rho}_{\boldsymbol{k}}\, \mathrm{e}^{i\boldsymbol{k}\cdot\boldsymbol{r}+st} + \rho_0 \tag{7}$$

$$\boldsymbol{v}(\boldsymbol{r},t) = \tilde{\boldsymbol{v}}_{\boldsymbol{k}}\, \mathrm{e}^{i\boldsymbol{k}\cdot\boldsymbol{r}+st} \tag{8}$$

$$T(\boldsymbol{r},t) = \tilde{T}_{\boldsymbol{k}}\, \mathrm{e}^{i\boldsymbol{k}\cdot\boldsymbol{r}+st} + T_0 \tag{9}$$

These spatially periodic solutions are known as the hydrodynamic modes. The decay rates $-s$ of these solutions are obtained by solving an eigenvalue problem for the five linearized hydrodynamic equations. These decay rates define the so-called dispersion relations of the five hydrodynamic modes. The dispersion relations can be expanded in powers of the wavenumber $k$ as shown in Table I. The sound modes are propagative because their dispersion relations include the imaginary term $\pm iU_sk$ with the sound velocity

$$U_s = \sqrt{\left(\frac{\partial P}{\partial \rho}\right)_s} \tag{10}$$

The shear and thermal modes are not propagative. All the hydrodynamic modes are damped with a relaxation rate proportional to the square of the wavenumber so that their damping vanishes as the wavelength of the mode tends to infinity, which has its origin in the fact that these five modes are associated with the five conserved quantities: mass, linear momenta, and energy. The damping coefficient of the sound modes is given by

$$\Gamma = \frac{1}{2\rho_0}\left[\left(\frac{1}{c_V} - \frac{1}{c_P}\right)\kappa + \frac{4}{3}\eta + \zeta\right] \tag{11}$$

where $c_V$ and $c_P$ are the specific heat capacities at constant volume and pressure, respectively [4].

The dispersion relations of the five hydrodynamic modes are depicted in Fig. 1. Beyond the hydrodynamic modes, there may exist kinetic modes that are not associated with conservation laws so that their decay rate does not vanish with the wavenumber. These kinetic modes are not described by the hydrodynamic equations but by the Boltzmann equation in dilute fluids. The decay rates of the kinetic modes are of the order of magnitude of the inverse of the intercollisional time.

A major preoccupation of nonequilibrium statistical mechanics is to justify the existence of the hydrodynamic modes from the microscopic Hamiltonian dynamics. Boltzmann equation is based on approximations valid for dilute fluids such as the Stosszahlansatz. In the context of Boltzmann's theory, the concept of hydrodynamic modes has a limited validity because of this approximation. We may wonder if they can be justified directly from the microscopic dynamics without any approximation. If this were the case, this would be great progress since it would prove that the irreversible relaxation toward the equilibrium state is ruled by decaying modes that are truly intrinsic

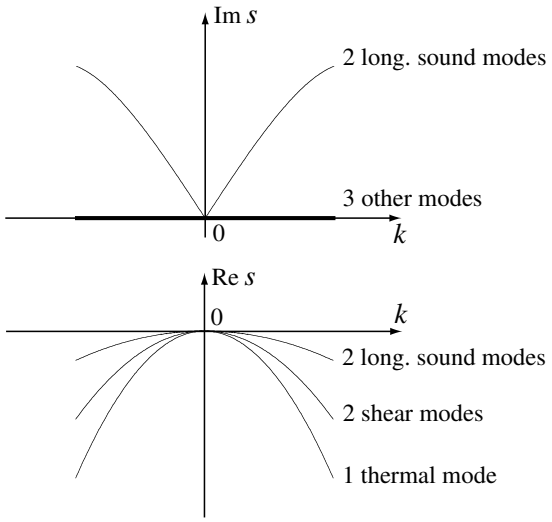


FIG. 1: Schematic dispersion relations of the five hydrodynamic modes of a fluid with one component.

to the microscopic Hamiltonian dynamics. Since the hydrodynamic modes decay exponentially, their microscopic construction would introduce time asymmetry into the statistical description and prove that irreversible processes can be deduced from the underlying Hamiltonian dynamics. We shall show in the following that dynamical systems theory has brought this extraordinary conceptual progress.

### B. Reaction-diffusion processes

Similar considerations concern the irreversible processes of diffusion and reaction in mixtures [5]. A system of $M$ different molecular species is described by the three components of velocity, the mass density, the temperature, and $(M-1)$ chemical concentrations and is ruled by $M+4$ partial differential equations. The $M-1$ extra equations govern the mutual diffusions and the possible chemical reactions $\rho = 1, 2, ..., R$

$$\sum_{a=1}^{M} \nu_a^{<\rho} \, \mathrm{X}_a \underset{w_{-\rho}}{\overset{w_{+\rho}}{\rightleftharpoons}} \sum_{a=1}^{M} \nu_a^{\rho>} \, \mathrm{X}_a \tag{12}$$

between the $M$ molecular species $\{\mathrm{X}_a\}_{a=1}^{M}$. The stoichiometric coefficients

$$\nu_a^{\rho} \equiv \nu_a^{\rho>} - \nu_a^{<\rho} = -\nu_a^{-\rho} \tag{13}$$

give the number of molecules of the species $a$ produced during the reaction $\rho$. The speed $w_\rho$ of the reaction $\rho$ is defined as the number of reactive events per unit time and is determined by the chemical concentrations of the molecules participating in the reaction. Each reaction $\rho$ is balanced by a reversed reaction $-\rho$, unless the reaction $\rho$ is fully irreversible in which case the reversed reaction has vanishing speed $w_{-\rho} = 0$. The chemical concentrations can be represented by the numbers of molecules per unit volume – that is, the particle densities $\{n_a\}_{a=1}^{M}$.

For an isothermal process, the chemical concentrations obey reaction-diffusion equations

$$\partial_t \, n_a = -\boldsymbol{\nabla} \cdot (n_a \boldsymbol{v} + \boldsymbol{J}_a) + \sum_{\rho=1}^{R} \nu_a^{\rho} \, w_\rho \tag{14}$$

with $a = 1, 2, ..., M$. The diffusive currents $\boldsymbol{J}_a$ are defined with respect to the center of mass of each fluid element so that they satisfy the constraint

$$\sum_{a=1}^{M} m_a \boldsymbol{J}_a = 0 \tag{15}$$

where $m_a$ is the mass of the molecule of species $a$. This constraint shows that the number of independent diffusive currents is limited to $M-1$. Accordingly, only $M-1$ mutual diffusions can exist in a fluid with $M$ components. Mutual diffusion is absent in a one-component fluid and becomes possible in a binary mixture.

A simple example of reaction is the isomerization

$$\mathrm{A} \underset{w_-}{\overset{w_+}{\rightleftharpoons}} \mathrm{B} \tag{16}$$

ruled by the coupled equations

$$\partial_t\, n_\mathrm{A} + \boldsymbol{\nabla}\cdot\boldsymbol{J}_\mathrm{A} \;=\; -w_+ + w_- \tag{17}$$
$$\partial_t\, n_\mathrm{B} + \boldsymbol{\nabla}\cdot\boldsymbol{J}_\mathrm{B} \;=\; +w_+ - w_- \tag{18}$$

We notice that the total mass is conserved because the mass density $\rho = m_\mathrm{A} n_\mathrm{A} + m_\mathrm{B} n_\mathrm{B}$ obeys the continuity equation

$$\partial_t\, \rho + \boldsymbol{\nabla}\cdot\boldsymbol{J} = 0 \tag{19}$$

with the mass current density $\boldsymbol{J} = m_\mathrm{A}\boldsymbol{J}_\mathrm{A} + m_\mathrm{B}\boldsymbol{J}_\mathrm{B}$.

In a dilute mixture, the reaction speeds are proportional to the chemical concentrations

$$w_+ \;\simeq\; \kappa_+\, n_\mathrm{A} \tag{20}$$
$$w_- \;\simeq\; \kappa_-\, n_\mathrm{B} \tag{21}$$

If cross-diffusion due to the chemical reaction is neglected, the diffusive currents are proportional to the gradients of concentrations

$$\boldsymbol{J}_\mathrm{A} \;\simeq\; -\mathcal{D}_\mathrm{A}\,\boldsymbol{\nabla} n_\mathrm{A} \tag{22}$$
$$\boldsymbol{J}_\mathrm{B} \;\simeq\; -\mathcal{D}_\mathrm{B}\,\boldsymbol{\nabla} n_\mathrm{B} \tag{23}$$

and we get the coupled reaction-diffusion equations

$$\partial_t\, n_\mathrm{A} \;=\; \mathcal{D}_\mathrm{A}\,\nabla^2 n_\mathrm{A} - \kappa_+\, n_\mathrm{A} + \kappa_-\, n_\mathrm{B} \tag{24}$$
$$\partial_t\, n_\mathrm{B} \;=\; \mathcal{D}_\mathrm{B}\,\nabla^2 n_\mathrm{B} + \kappa_+\, n_\mathrm{A} - \kappa_-\, n_\mathrm{B} \tag{25}$$

These equations are linear and their general solution is given by the linear combination of spatially periodic modes

$$n_\mathrm{A}(\boldsymbol{r},t) \;=\; \tilde{n}_{\mathrm{A},\boldsymbol{k}}\; \mathrm{e}^{i\boldsymbol{k}\cdot\boldsymbol{r}+st} + n_{\mathrm{A},0} \tag{26}$$
$$n_\mathrm{B}(\boldsymbol{r},t) \;=\; \tilde{n}_{\mathrm{B},\boldsymbol{k}}\; \mathrm{e}^{i\boldsymbol{k}\cdot\boldsymbol{r}+st} + n_{\mathrm{B},0} \tag{27}$$

The system admits two kinds of modes. The diffusive mode has the dispersion relation

$$s = -\mathcal{D}\,k^2 + O(k^4) \tag{28}$$

with the diffusion coefficient

$$\mathcal{D} = \frac{\kappa_+\mathcal{D}_\mathrm{B} + \kappa_-\mathcal{D}_\mathrm{A}}{\kappa_+ + \kappa_-} \tag{29}$$

The diffusive mode is associated with the conservation (19) of the total mass since its dispersion relation vanishes with the wavenumber. Besides, we find a reactive mode with the dispersion relation

$$s = -\kappa_+ - \kappa_- - \mathcal{D}^{(\mathrm{r})}\,k^2 + O(k^4) \tag{30}$$

which does not vanish with the wavenumber. The associated reactive diffusion coefficient is given by

$$\mathcal{D}^{(\mathrm{r})} = \frac{\kappa_+\mathcal{D}_\mathrm{A} + \kappa_-\mathcal{D}_\mathrm{B}}{\kappa_+ + \kappa_-} \tag{31}$$

The dispersion relations of the two modes are depicted in Fig. 2. The reactive mode is one of the kinetic modes existing beside the hydrodynamic modes such as the diffusive mode. Here also, we may wonder if these modes can be justified from the microscopic dynamics.

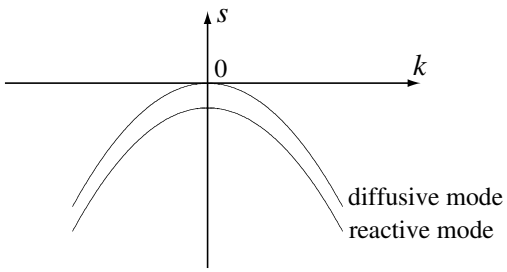


FIG. 2: Schematic dispersion relations of the diffusive and reactive modes of the reaction of isomerization $A \rightleftharpoons B$ taking place in a solvent at rest.

### C. Nonequilibrium thermodynamics

The second law of thermodynamics asserts that the total entropy $S$ of a system may change in time because of exchanges with its environment and internal entropy production which is vanishing at equilibrium and positive out of equilibrium [5]

$$\frac{dS}{dt} = \frac{d_{\rm e}S}{dt} + \frac{d_{\rm i}S}{dt} \qquad \text{with} \quad \frac{d_{\rm i}S}{dt} \geq 0 \tag{32}$$

The second law can be expressed in terms of the local balance equation for the entropy:

$$\partial_t\, \rho s = -\boldsymbol{\nabla}\cdot\boldsymbol{J}_s + \sigma_s \tag{33}$$

The entropy is given in terms of the specific entropy $s$ by $S = \int \rho s\, d^3r$ so that the entropy flux out of the system is related to the entropy current density by

$$\frac{d_{\rm e}S}{dt} = \int \boldsymbol{J}_s \cdot d\boldsymbol{\Sigma} \tag{34}$$

and the entropy production to the entropy source by

$$\frac{d_{\rm i}S}{dt} = \int \sigma_s\, d^3r \geq 0 \tag{35}$$

The entropy production is due to the contributions of the different irreversible processes taking place in the system. The entropy source is given by the sum [5]

$$\sigma_s = \sum_\alpha A_\alpha\, J_\alpha \geq 0 \tag{36}$$

of the affinities or thermodynamic forces $A_\alpha$ [6] multiplied by the currents $J_\alpha$ associated with each one of these irreversible processes listed in Table II. In the linear regime, Onsager has assumed that the currents are proportional to the affinities [7]:

$$J_\alpha \simeq \sum_\beta L_{\alpha\beta} A_\beta \tag{37}$$

The microscopic justification of the second law of thermodynamics has always been a major problem in nonequilibrium statistical mechanics. Recent work has shown that it is possible to derive *ab initio* the entropy production thanks to the construction of the hydrodynamic modes [8, 9]. As shown by Boltzmann, the entropy is an extra-mechanical quantity that characterizes the disorder of the system at a given time. It is therefore related to the probability distribution describing the statistical state of the system. The characterization of the disorder requires the counting of the number of possible microstates corresponding to a given probability distribution. This counting is possible if discrete coarse-grained states are defined for this purpose as proposed by Gibbs in 1902 [10]. This coarse graining has been further justified by quantum mechanics which showed that the discrete states must be identified with phase-space cells of volume $\Delta^f r \Delta^f p = (2\pi\hbar)^f$, as done in the Sackur-Tetrode formula. In this way, a natural definition can be given to the entropy even in nonequilibrium states. Gibbs coarse-grained entropy has been in agreement with the experimental measures of entropy for a century. As explained below, it is possible to derive the entropy production (36) of nonequilibrium thermodynamics thanks to the recent advances in dynamical systems theory and, in particular, the construction of the hydrodynamic modes at the microscopic level of description.

TABLE II: Different irreversible processes with their affinity or thermodynamic force $A_\alpha$ and their current $J_\alpha$. $T$ is the temperature, $v_i$ the fluid velocity, $\mathit{\Pi}_{ij}$ the viscous pressure tensor, $\boldsymbol{J}_q$ the heat current density, $\mu_a$ its chemical potential, $\boldsymbol{J}_a$ the current density of molecular species $a$, $\nu_a^\rho$ the stoichiometric coefficient (13), and $w_\rho$ the speed of reaction $\rho$.

| irreversible process ($\alpha$) | affinity $A_\alpha$ | current $J_\alpha$ |
|---|---|---|
| shear viscosity ($\eta$) | $-\frac{1}{2T}\left(\nabla_i v_j + \nabla_j v_i - \frac{2}{3}\boldsymbol{\nabla}\cdot\boldsymbol{v}\,\delta_{ij}\right)$ | $\mathit{\Pi}_{ij} - \frac{1}{3}\,\mathrm{tr}\boldsymbol{\mathit{\Pi}}\,\delta_{ij}$ |
| bulk viscosity ($\zeta$) | $-\frac{1}{3T}\boldsymbol{\nabla}\cdot\boldsymbol{v}\,\delta_{ij}$ | $\frac{1}{3}\,\mathrm{tr}\boldsymbol{\mathit{\Pi}}\,\delta_{ij}$ |
| heat conduction ($\kappa$) | $\boldsymbol{\nabla}\frac{1}{T}$ | $\boldsymbol{J}_q$ |
| diffusion ($\mathcal{D}$) | $-\boldsymbol{\nabla}\frac{\mu_a}{T}$ | $\boldsymbol{J}_a$ |
| reaction ($L$) | $-\frac{1}{T}\sum_{a=1}^{M}\nu_a^\rho\mu_a$ | $w_\rho$ |

## III. MICROREVERSIBILITY AND TIME ASYMMETRY

A major preoccupation in nonequilibrium statistical mechanics is to derive hydrodynamics and nonequilibrium thermodynamics from the microscopic Hamiltonian dynamics of the particles composing matter. The positions $\{\boldsymbol{r}_a\}_{a=1}^N$ and momenta $\{\boldsymbol{p}_a\}_{a=1}^N$ of these particles obey Newton's equations or, equivalently, Hamilton's equations:

$$\frac{d\boldsymbol{r}_a}{dt} = +\frac{\partial H}{\partial \boldsymbol{p}_a} \tag{38}$$

$$\frac{d\boldsymbol{p}_a}{dt} = -\frac{\partial H}{\partial \boldsymbol{r}_a} \tag{39}$$

Since the Hamiltonian function $H$ is an even function of the momenta, Hamilton's equation are symmetric under time reversal:

$$\boldsymbol{\Theta}\left(\boldsymbol{r}_1,\boldsymbol{r}_2,...,\boldsymbol{r}_N,\boldsymbol{p}_1,\boldsymbol{p}_2,...,\boldsymbol{p}_N,t\right) = \left(\boldsymbol{r}_1,\boldsymbol{r}_2,...,\boldsymbol{r}_N,-\boldsymbol{p}_1,-\boldsymbol{p}_2,...,-\boldsymbol{p}_N,-t\right) \tag{40}$$

Furthermore, the phase-space volumes are preserved during the Hamiltonian time evolution, according to Liouville's theorem. We denote by

$$\boldsymbol{\mathit{\Gamma}} = \left(\boldsymbol{r}_1,\boldsymbol{r}_2,...,\boldsymbol{r}_N,\boldsymbol{p}_1,\boldsymbol{p}_2,...,\boldsymbol{p}_N\right) \in \mathcal{M} \tag{41}$$

a point in the phase space $\mathcal{M}$ of positions and momenta and by

$$\boldsymbol{\mathit{\Gamma}}_t = \boldsymbol{\Phi}^t(\boldsymbol{\mathit{\Gamma}}_0) \tag{42}$$

the unique solution of Hamilton's equations starting from the initial condition $\boldsymbol{\mathit{\Gamma}}_0$.

The time-reversal symmetry of the Hamiltonian dynamics, also called the microreversibility, is the property that if the phase-space trajectory

$$\mathcal{C} = \{\boldsymbol{\mathit{\Gamma}}_t = \boldsymbol{\Phi}^t(\boldsymbol{\mathit{\Gamma}}_0) : t \in \mathbb{R}\} \tag{43}$$

is a solution of Hamilton's equations, then its time reversal

$$\boldsymbol{\Theta}(\mathcal{C}) = \{\tilde{\boldsymbol{\mathit{\Gamma}}}_{t'} = \boldsymbol{\Phi}^{t'} \circ \boldsymbol{\Theta}(\boldsymbol{\mathit{\Gamma}}_0) : t' \in \mathbb{R}\} \tag{44}$$

is also a solution of Hamilton's equations. It is not often emphasized that, typically, the trajectory and its time reversal are physically distinct trajectories

$$\mathcal{C} \neq \boldsymbol{\Theta}(\mathcal{C}) \tag{45}$$

and that it is rather exceptional that they coincide (as in the case of a harmonic oscillator). Already for a free particle of Newton's equation $d^2x/dt^2 = 0$, the trajectory $x = v_0t + x_0$ is physically distinct from its time reversal $x = -v_0t + x_0$ unless $v_0 = 0$. This remark shows that the solutions of Hamilton's equations do not necessarily have the time-reversal symmetry of the set of equations itself. This phenomenon is well known under the name of spontaneous symmetry breaking and is common in condensed matter physics. In this regard, we notice that it is a major historical development that Newton and his followers have conceptually separated the actual trajectory of a system of interest from the fundamental equation of motion which rules all the possible trajectories given by its solutions. The microreversibility is the time-reversal symmetry of the set of all the possible solutions of Newton's equations but this does not imply the time-reversal symmetry of the unique trajectory followed by the Universe. Most of the solutions of typical Newton's equations break the time-reversal symmetry of the equations. In this perspective, the Newtonian scheme appears to be compatible with the possibility of irreversible time evolutions if irreversibility is understood as the property of the trajectory (as in pre-Newtonian science) and not with the fundamental equations of motion. Today, we are familiar with such phenomena of spontaneous symmetry breaking according to which the solution of an equation may have a lower symmetry than the equation itself. It is our purpose to show that irreversibility can be understood in a similar way as a spontaneous breaking of the time-reversal symmetry at the statistical level of description.

## IV. POLLICOTT-RUELLE RESONANCES AND TIME-REVERSAL SYMMETRY BREAKING

Modern dynamical systems theory has shown that the solutions of Newton's equations may be as random as a coin tossing probability game. A mechanism allowing such a dynamical randomness is the sensitivity to initial conditions of chaotic dynamical systems. This mechanism can conciliate causality and determinism with the existence of random events. Causality says that each effect has a cause and determinism that a unique cause can be associated to each effect once a system is described in its globability. In constrast, we observe in nature many random events as effects without apparent causes. Maxwell and Poincaré have judiciously pointed out that there exist systems with sensitivity to initial conditions in which small causes can lead to big effects. If the cause is so minute that it went unnoticed, such a deterministic dynamics can therefore explain a random or stochastic process. Most remarkably, there exists today a quantitative theory for such properties as dynamical randomness and sensitivity to initial conditions. The historical milestones are the following: Dynamical randomness has been first characterized by the information theory of Shannon around 1948 [11]. The quantitative characterization of dynamical randomness was established in the work of Kolmogorov and Sinai in 1959 with the concept of entropy per unit time [12, 13]. This latter characterizes the disorder of the trajectories along the time axis, while the thermodynamic entropy is a measure of disorder in space at a given time; otherwise, both entropies have similar interpretations. On the other hand, the concept of Lyapunov exponents was introduced to describe quantitatively the sensitivity to initial conditions [14], which Lorenz discovered in the context of meteorology in 1963 [15]. The Lyapunov exponents are defined as the rates of exponential separation between a reference trajectory and a perturbed one:

$$\lambda_i = \lim_{t\to\infty} \frac{1}{t} \ln \frac{\|\delta \boldsymbol{\Gamma}_i(t)\|}{\|\delta \boldsymbol{\Gamma}_i(0)\|} \tag{46}$$

where $\delta\boldsymbol{\Gamma}_i(t)$ denotes the infinitesimal perturbation at time $t$ on the reference trajectory. There exist as many Lyapunov exponents as there are directions $i = 1, 2, ..., 2f = 6N$ in the phase space. In 1977, Pesin proved that dynamical randomness finds its origin in the sensitivity to initial conditions [16]. Thereafter, fundamental connections between these new concepts from dynamical systems theory and nonequilibrium statistical mechanics have been discovered since 1990 [1].

It is essential to understand that the aforementioned dynamical randomness is quantitatively comparable to the one seen in Brownian motion or other stochastic processes of nonequilibrium statistical mechanics. Indeed, the dynamical randomness of the stochastic processes can also be characterized by a positive entropy per unit time. Since the mid nineties, we can compute the Kolmogorov-Sinai entropy per unit time as well as the spectrum of Lyapunov exponents is the many-particle systems of statistical mechanics such as the hard-sphere gas [17–19]. In a dilute gas, a typical Lyapunov exponent is of the order of the inverse of the intercollisional time and the Kolmogorov-Sinai entropy per unit time of the order of the Avogadro number multiplied by a typical Lyapunov exponent, showing that many-particle systems have a huge dynamical randomness [1].

Figure 3 depicts the spectrum of Lyapunov exponents in a hard-sphere system. The area below the positive Lyapunov exponent gives the value of the Kolmogorov-Sinai entropy per unit time. The positive Lyapunov exponents show that the typical trajectories are dynamically unstable. There are as many phase-space directions in which a perturbation can amplify as there are positive Lyapunov exponents. All these unstable directions are mapped onto corresponding stable directions by the time-reversal symmetry. However, the unstable phase-space directions

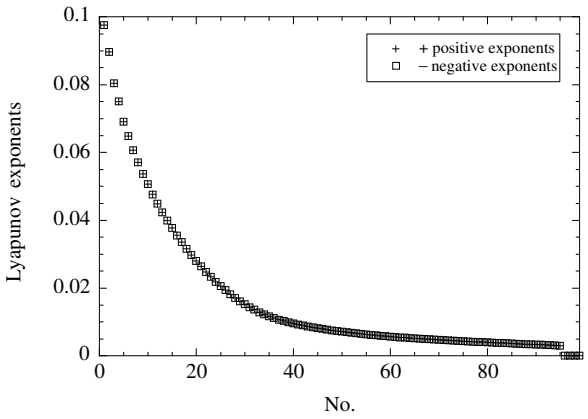


FIG. 3: Spectrum of Lyapunov exponents of a dynamical system of 33 hard spheres of unit diameter and mass at unit temperature and density 0.001. The positive Lyapunov exponents are superposed to minus the negative ones showing that the Lyapunov exponents come in pairs $\{\lambda_i, -\lambda_i\}$ as expected in Hamiltonian systems. Eight Lyapunov exponents vanish because the system has four conserved quantities, namely, energy and the three components of momentum and because of the pairing rule. The total number of Lyapunov exponents is equal to $6 \times 33 = 198$.

are physically distinct from the stable ones. Therefore, systems with positive Lyapunov exponents are especially propitious for the spontaneous breaking of the time-reversal symmetry, as shown below.

The Lyapunov exponents and the Kolmogorov-Sinai entropy per unit time concern the short time scale of the kinetics of collisions taking place in the fluid. The longer time scales of the hydrodynamics are instead characterized by the decay of the statistical averages or the time correlation functions of the observables. Here, we consider a statistical ensemble of trajectories described by a probability density $p(\boldsymbol{\Gamma})$, which is known to evolve in time according to the famous Liouville equation of nonequilibrium statistical mechanics [4]:

$$\partial_t\, p = \hat{L} p \tag{47}$$

The Liouvillan operator is defined in terms of the Poisson bracket with the Hamiltonian:

$$\hat{L} \equiv \{H,\ \} = \sum_{a=1}^{N} \left( \frac{\partial H}{\partial \boldsymbol{r}_a} \cdot \frac{\partial}{\partial \boldsymbol{p}_a} - \frac{\partial H}{\partial \boldsymbol{p}_a} \cdot \frac{\partial}{\partial \boldsymbol{r}_a} \right) \tag{48}$$

The time evolution of the probability density is induced by Hamiltonian dynamics so that it has its properties, in particular, the time-reversal symmetry. However, the solutions of Liouville's equation can also break this symmetry as it is the case for Newton's equations. This is the case if each trajectory (43) has a different probability weight than its time reversal (44) and that both are physically distinct (45).

The idea of Pollicott-Ruelle resonances relies on this mechanism of spontaneous breaking of the time-reversal symmetry [20, 21]. The Pollicott-Ruelle resonances are generalized eigenvalues $s_j$ of Liouvillian operator associated with decaying eigenstates which are singular in the stable phase-space directions but smooth in the unstable ones:

$$\hat{L} \Psi_j = s_j \Psi_j \tag{49}$$

These are the classical analogues of quantum scattering resonances except that these latter ones are associated with the wave eigenfunctions of the energy operator although the eigenstates of the Liouvillian operator are probability densities or density matrices in quantum mechanics. Nevertheless, the mathematical method to determine the Pollicott-Ruelle resonances is similar and they can be obtained as poles of the resolvent of the Liouvillian operator

$$\frac{1}{s - \hat{L}} \tag{50}$$

at real or complex values of the variable $s$ which is a complex frequency. The poles can thus be identified by analytic continuation of the resolvent toward complex frequencies. This idea has already been proposed in the early sixties in the context of nonequilibrium statistical mechanics [4]. In the mid-eighties, Pollicott and Ruelle provides rigorous and systematic tools in order to determine these resonances in fully chaotic systems [20, 21]. The periodic-orbit theory

was developed which clearly showed that these resonances are intrinsic to the dynamics of the system [1, 22]. The knowledge of these resonances allows us to decompose the time evolution of the statistical averages of the observables

$$\langle A\rangle_t = \langle A|\exp(\hat{L}t)|p_0\rangle = \int A(\boldsymbol{\Phi}^t\boldsymbol{\Gamma}_0)\; p_0(\boldsymbol{\Gamma}_0)\; d\boldsymbol{\Gamma}_0 = \int A(\boldsymbol{\Gamma})\; p_t(\boldsymbol{\Gamma})\; d\boldsymbol{\Gamma} \tag{51}$$

into decaying exponential functions. The resonances obtained by analytic continuation toward negative values of $\mathrm{Re}\, s$ are associated with exponential decays for positive times (see Fig. 4). The corresponding expansion defines the forward semigroup:

$$\langle A\rangle_t = \langle A|\exp(\hat{L}t)|p_0\rangle \simeq \sum_j \langle A|\Psi_j\rangle\; \exp(s_j t)\; \langle\tilde{\Psi}_j|p_0\rangle + \cdots \tag{52}$$

which is only valid for $t > 0$. The dots denote the contributions beside the simple exponentials due to the resonances. These extra contributions may include Jordan-block structures if a resonance has a multiplicity $m_j$ higher than unity. In this case, the exponential decay is modified by a power-law dependence on time as $t^{m_j-1}\mathrm{e}^{s_j t}$ [1]. It is important to notice that the expansion (52) is obtained without assuming that the Liouvillian operator is anti-Hermitian so that the right-hand eigenstate $\Psi_j$ will in general differ from the left-hand eigenstate $\tilde{\Psi}_j$. As a corollary, these eigenstates do not belong to a Hilbert space of square integrable functions, instead they can be singular distributions. In particular, the right-hand eigenstates associated with nonvanishing eigenvalue $s_j \neq 0$ are smooth in the unstable phase-space directions but singular in the stable ones. On long time scales, the statistical average (52) tends toward the slowest decay with the eigenvalue for which $|\mathrm{Re}\, s_j|$ is minimum (see Fig. 5). If this eigenvalue is $s_0 = 0$, the statistical average converges toward a stationary state which defines the state of thermodynamic equilibrium. Here, we recover the fundamental property of mixing introduced by Gibbs in 1902 according to which the statistical averages and the time correlation functions weakly converge toward their equilibrium value [10].

On the other hand, the antiresonances obtained by analytic continuation toward positive values of $\mathrm{Re}\, s$ are associated with exponential decays for negative times. The corresponding expansion defines the backward semigroup:

$$\langle A\rangle_t = \langle A|\exp(\hat{L}t)|p_0\rangle \simeq \sum_j \langle A|\Psi_j\circ\boldsymbol{\Theta}\rangle\; \exp(-s_j t)\; \langle\tilde{\Psi}_j\circ\boldsymbol{\Theta}|p_0\rangle + \cdots \tag{53}$$

valid for $t < 0$ (see Fig. 5).

We notice that it is the analytic continuation which has the effect of breaking the time-reversal symmetry. If we contented ourselves with the continuous spectrum of eigenvalues with $\mathrm{Re}\, s = 0$, we would obtain the unitary group of time evolution valid for positive and negative times. The unitary spectral decomposition is as valid as the spectral decompositions of the forward or backward semigroups. However, only the semigroups provide us with well defined relaxation rates that are intrinsic to the system. The continuous spectrum of the unitary group does not display characteristic times.

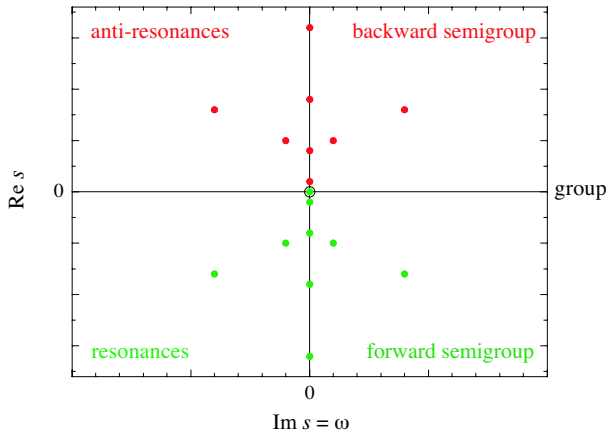


FIG. 4: Complex plane of the variable $s$. The vertical axis $\mathrm{Re}\, s$ is the axis of the rates or complex frequencies. The horizontal axis $\mathrm{Im}\, s$ is the axis of real frequencies $\omega$. The resonances are the poles in the lower half-plane contributing to the forward semigroup. The antiresonances are the poles in the upper half-plane contributing to the backward semigroup. The resonances are mapped onto the antiresonances by time reversal. Complex singularities such as branch cuts are also possible but not depicted here. The spectrum contributing to the unitary group of time evolution is found on the axis $\mathrm{Re}\, s = 0$.

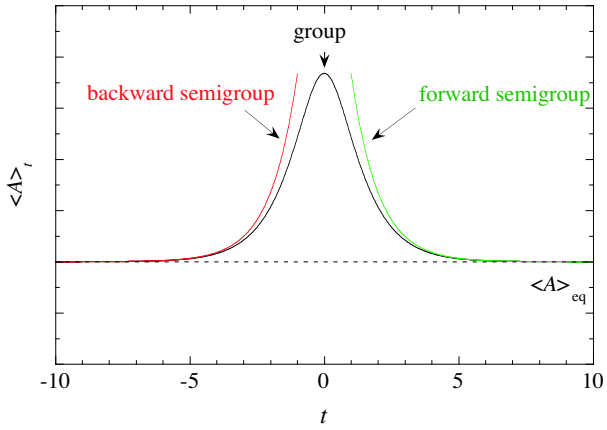


FIG. 5: Time evolution of the statistical average (51) according to the expansion (52) of the forward semigroup valid for $t > 0$ and the expansion (53) of the backward semigroup valid for $t < 0$.

## V. MICROSCOPIC CONSTRUCTION OF THE DIFFUSIVE MODES

### A. The diffusive modes as Liouvillian eigenstates

When applied to spatially extended dynamical systems, the Pollicott-Ruelle resonances give the dispersion relations of the hydrodynamic and kinetic modes of relaxation toward the equilibrium state. This can be illustrated in models of deterministic diffusion such as the multibaker map, the hard-disk Lorentz gas, or the Yukawa-potential Lorentz gas [1, 23]. These systems are spatially periodic. Their time evolution Frobenius-Perron operator

$$\hat{P}^t = \exp(\hat{L}t) \tag{54}$$

is invariant under a discrete group of spatial translations $\hat{T}^{\boldsymbol{a}}$:

$$\left[\hat{P}^t, \hat{T}^{\boldsymbol{a}}\right] = 0 \tag{55}$$

Since these operators commute, they admit common eigenstates:

$$\hat{P}^t \Psi_{\boldsymbol{k}} = \exp(s_{\boldsymbol{k}} t)\Psi_{\boldsymbol{k}} \tag{56}$$

$$\hat{T}^{\boldsymbol{a}} \Psi_{\boldsymbol{k}} = \exp(i\boldsymbol{k}\cdot\boldsymbol{a})\Psi_{\boldsymbol{k}} \tag{57}$$

The generalized eigenvalue $s_{\boldsymbol{k}}$ is a Pollicott-Ruelle resonance associated with the eigenstate $\Psi_{\boldsymbol{k}}$. The hydrodynamic modes can be identified as the eigenstates associated with eigenvalues $s_{\boldsymbol{k}}$ vanishing with the wavenumber $\boldsymbol{k}$.

Here, we consider the diffusive processes in which independent particles are transported in a lattice where they perform a random walk. According to a formula by Van Hove [24], the dispersion relation of diffusion is given by

$$s_{\boldsymbol{k}} = \lim_{t\to\infty} \frac{1}{t} \ln\langle \exp\left[i\boldsymbol{k}\cdot(\boldsymbol{r}_t - \boldsymbol{r}_0)\right]\rangle = -\mathcal{D}\boldsymbol{k}^2 + O(\boldsymbol{k}^4) \tag{58}$$

where $\boldsymbol{r}_t$ is the position of the particle in the lattice. The diffusion coefficient $\mathcal{D}$ is obtained by expanding in powers of the wavenumber and is given by Einstein and Green-Kubo formulas [25, 26]. The dispersion relation of diffusion (58) is nothing other than a Liouvillian eigenvalue and should therefore be found among the Pollicott-Ruelle resonances of the dynamical system. The corresponding diffusive mode has the wavelength $2\pi/\|\boldsymbol{k}\|$ and decays exponentially at the rate $-s_{\boldsymbol{k}}$ as depicted in Fig. 6.

At the microscopic level of description, the hydrodynamic mode of diffusion is defined as the Liouvillian eigenstate:

$$\hat{L}\Psi_{\boldsymbol{k}} = s_{\boldsymbol{k}}\,\Psi_{\boldsymbol{k}} \tag{59}$$

Since this latter is expected to be a singular distribution, its density $\Psi_{\boldsymbol{k}}$ cannot be depicted as a function. Accordingly, we consider its cumulative function by integrating over some curve in phase space. This curve is followed by changing the parameter $\theta$:

$$F_{\boldsymbol{k}}(\theta) = \lim_{t\to\infty} \frac{\int_0^\theta d\theta' \exp\left[i\boldsymbol{k}\cdot(\boldsymbol{r}_t - \boldsymbol{r}_0)_{\theta'}\right]}{\int_0^{2\pi} d\theta' \exp\left[i\boldsymbol{k}\cdot(\boldsymbol{r}_t - \boldsymbol{r}_0)_{\theta'}\right]} \tag{60}$$

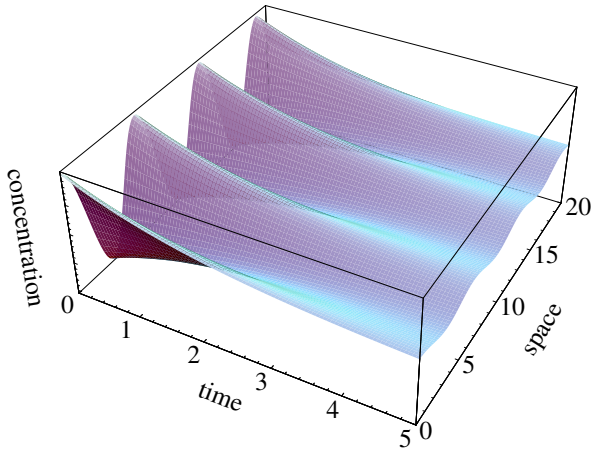


FIG. 6: Schematic representation of the relaxation of a diffusive mode in space and time toward the uniform equilibrium state.

This function is normalized to take the unit value for $\theta = 2\pi$. For vanishing wavenumber, the cumulative function is equal to $F_{\boldsymbol{k}}(\theta) = \theta/(2\pi)$, which is the cumulative function of the microcanonical uniform distribution in phase space. For nonvanishing wavenumbers, the cumulative function becomes complex. These cumulative functions typically form fractal curves in the complex plane $(\mathrm{Re}\, F_{\boldsymbol{k}}, \mathrm{Im}\, F_{\boldsymbol{k}})$. Their Hausdorff dimension $D_{\mathrm{H}}$ can be calculated as follows. We can decompose the phase space into cells labeled by $\omega$ and represent the trajectories by the sequence $\boldsymbol{\omega} = \omega_0\omega_1\omega_2...\omega_{n-1}$ of cells visited at regular time interval $0, \tau, 2\tau, ..., (n-1)\tau$. The integral over the phase-space curve in Eq. (60) can be discretized into a sum over the paths $\boldsymbol{\omega}$. The weight of each path $\boldsymbol{\omega}$ is inversely proportional to the stretching factor $\Lambda(\boldsymbol{\omega})$ by which perturbations are amplified due to the dynamical instability in the phase space so that we get

$$F_{\boldsymbol{k}}(\theta) = \lim_{n\to\infty} \sum_{\boldsymbol{\omega}} \frac{1}{|\Lambda(\boldsymbol{\omega})|}\, \mathrm{e}^{i\boldsymbol{k}\cdot(\boldsymbol{r}_{n\tau}-\boldsymbol{r}_0)_{\boldsymbol{\omega}}}\, \mathrm{e}^{-s_{\boldsymbol{k}}n\tau} = \lim_{n\to\infty} \sum_{\boldsymbol{\omega}} \Delta F_{\boldsymbol{k}}(\boldsymbol{\omega}) \tag{61}$$

where we have used the fact that the denominator in Eq. (60) behaves as $\exp(s_{\boldsymbol{k}}t)$. This provides the approximation of the cumulative function as a polygonal curve formed by a sequence of complex vectors. The Hausdorff dimension of this curve is obtained by the condition

$$\sum_{\boldsymbol{\omega}} |\Delta F_{\boldsymbol{k}}(\boldsymbol{\omega})|^{D_{\mathrm{H}}} \sim 1 \qquad \text{for} \quad n \to \infty \tag{62}$$

This condition can be rewritten in terms of Ruelle's function defined as the generating function of the Lyapunov exponents and their statistical moments:

$$P(\beta) \equiv \lim_{n\tau\to\infty} \frac{1}{n\tau} \ln \sum_{\boldsymbol{\omega}} \frac{1}{|\Lambda(\boldsymbol{\omega})|^{\beta}} \tag{63}$$

Combining Eqs. (61), (62), and (63), we finally obtain the formula:

$$P(D_{\mathrm{H}}) = D_{\mathrm{H}}\ \mathrm{Re}\ s_{\boldsymbol{k}} \tag{64}$$

which gives the Hausdorff dimension in terms of the dispersion relation of diffusion and Ruelle's function [23].

Since Ruelle's function vanishes if its argument takes the unit value $P(1) = 0$, the Hausdorff dimension can be expanded in powers of the wavenumber as

$$D_{\mathrm{H}}(\boldsymbol{k}) = 1 + \frac{\mathcal{D}}{\lambda}\, \boldsymbol{k}^2 + \mathcal{O}(\boldsymbol{k}^4) \tag{65}$$

so that the diffusion coefficient can be obtained from the Hausdorff dimension and the Lyapunov exponent by the formula

$$\mathcal{D} = \lambda \lim_{\boldsymbol{k}\to 0} \frac{D_{\mathrm{H}}(\boldsymbol{k}) - 1}{\boldsymbol{k}^2} \tag{66}$$

This formula has been verified for the following dynamical systems sustaining deterministic diffusion [23].

### B. Multibaker model of diffusion

One of the simplest models of deterministic diffusion is the multibaker map, which is a generalization of the well-known baker map into a spatially periodic system [1, 27, 28]. The map is two dimensional and rules the motion of a particle which can jump from square to square in a random walk. The equations of the map are given by

$$\phi(l,x,y) = \begin{cases} \left(l-1, 2x, \frac{y}{2}\right) , & 0 \le x \le \frac{1}{2} \\ \left(l+1, 2x-1, \frac{y+1}{2}\right) , & \frac{1}{2} < x \le 1 \end{cases} \tag{67}$$

where $(x, y)$ are the coordinates of the particle inside a square, while $l \in \mathbb{Z}$ is an integer specifying in which square the particle is currently located. This map acts as a baker map but, instead of mapping the two stretched halves into themselves, they are moved to the next-neighboring squares as shown in Fig. 7.

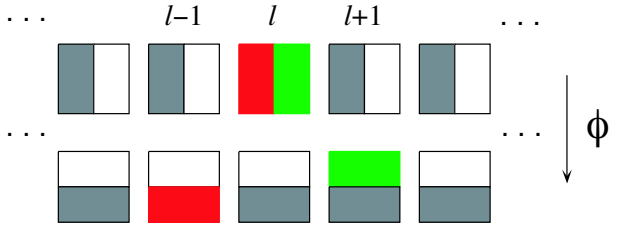


FIG. 7: Schematic representation of the multibaker map $\phi$ acting on an infinite sequence of squares.

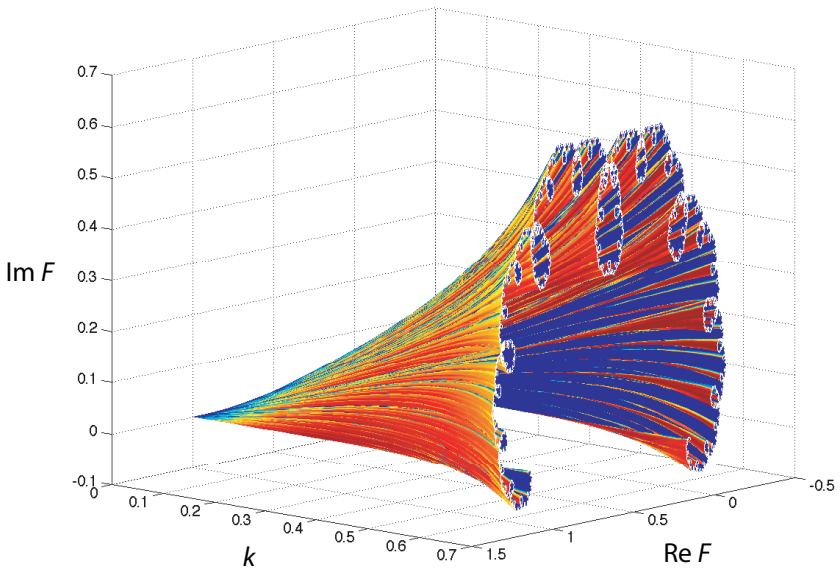


FIG. 8: The diffusive modes of the multibaker map represented by their cumulative function depicted in the complex plane $(\mathrm{Re}\, F_k, \mathrm{Im}\, F_k)$ versus the wavenumber $k$.

The multibaker map preserves the vertical and horizontal directions, which correspond respectively to the stable and unstable directions. Accordingly, the diffusive modes of the forward semigroup are horizontally smooth but vertically singular. Both directions decouple and it is possible to write down iterative equations for the cumulative functions of the diffusive modes, which are known as de Rham functions [1, 29]

$$F_k(y) = \begin{cases} \alpha F_k(2y) , & 0 \le y \le \frac{1}{2} \\ (1-\alpha) F_k(2y-1) + \alpha , & \frac{1}{2} < y \le 1 \end{cases} \tag{68}$$

with

$$\alpha = \frac{\exp(ik)}{2\cos k} \tag{69}$$

For each value of the wavenumber $k$, the de Rham functions depict fractal curves as seen in Fig. 8. The fractal dimension of these fractal curves can be calculated using Eq. (64). Since the multibaker map is equivalent to a random walk in a one-dimensional lattice with probabilities $\frac{1}{2}$ to jump to the left- or right-hand sides, the dispersion relation of diffusion is given by

$$s_k = \ln \cos k = -\frac{1}{2}k^2 + O(k^4) \tag{70}$$

so that the diffusion coefficient is equal to $\mathcal{D} = \frac{1}{2}$. Since the dynamics is uniformly expanding by a factor 2 in the multibaker map, Ruelle's function (63) has the form

$$P(\beta) = (1 - \beta) \ln 2 \tag{71}$$

whereupon the Hausdorff dimension of the diffusive mode takes the value

$$D_{\mathrm{H}} = \frac{\ln 2}{\ln 2 \cos k} \tag{72}$$

according to Eq. (64) [30].

### C. Periodic hard-disk Lorentz gas

The periodic hard-disk Lorentz gas is a two-dimensional billiard in which a point particle undergoes elastic collisions on hard disks which are fixed in the plane in the form of a spatially periodic lattice. Bunimovich and Sinai have proved that the motion is diffusive if the horizon seen by the particles is always finite [31]. This is the case for a hexagonal lattice under the condition that the disks are large enough to avoid the possibility of straight trajectories moving across the whole lattice without collision. The dynamics of this system is ruled by the free-particle Hamiltonian:

$$H = \frac{\boldsymbol{p}^2}{2m} \tag{73}$$

supplemented by the rules of elastic collisions on the disks. Because of the defocusing character of the collisions on the disks, the motion is chaotic. Two trajectories issued from slightly different initial conditions are depicted in Fig. 9. The dynamics is very sensitive to the initial conditions because the trajectories separate after a few collisions as seen in Fig. 9b. On long times, the trajectories perform random walks on the lattice (see Fig. 9a).

The cumulative functions of the diffusive modes can be constructed by using Eq. (60). The trajectories start from the border of a disk with an initial position at an angle $\theta$ with respect to the horizontal and an initial velocity normal to the disk. The result is depicted in Fig. 10, where we see the fractal character of these curves developing as the wavenumber $\boldsymbol{k}$ increases. The Hausdorff dimension satisfies Eq. (65) as shown elsewhere [23].

### D. Periodic Yukawa-potential Lorentz gas

This other Lorentz gas is similar to the previous one except that the hard disks are replaced by Yukawa potentials centered here at the vertices of a square lattice. The Hamiltonian of this system is given by

$$H = \frac{\boldsymbol{p}^2}{2m} - \sum_i \frac{\exp(-ar_i)}{r_i} \tag{74}$$

where $a$ is the inverse screening length. Knauf has proved that this system is chaotic and diffusive if the energy of the moving particles is large enough [32]. The sensitivity to initial conditions is illustrated in Fig. 11 which depicts two trajectories starting from very close initial conditions. The particles undergo a random walk on long time scales.

The cumulative functions of the diffusive modes can here also be constructed by using Eq. (60) with trajectories integrated with a numerical algorithm based on the rescaling of time at the singular collisions. The initial position is taken on a small circle around a scattering center at an angle $\theta$ with respect to the horizontal direction and the initial velocity is normal and pointing to the exterior of this circle. The results are shown in Fig. 12 for two nonvanishing wavenumbers. The Hausdorff dimension of these fractal curves also satisfies Eq. (65) as shown elsewhere [23].

Beside the diffusive modes, the chemical modes can also be constructed in models of reaction-diffusion processes [33–36].

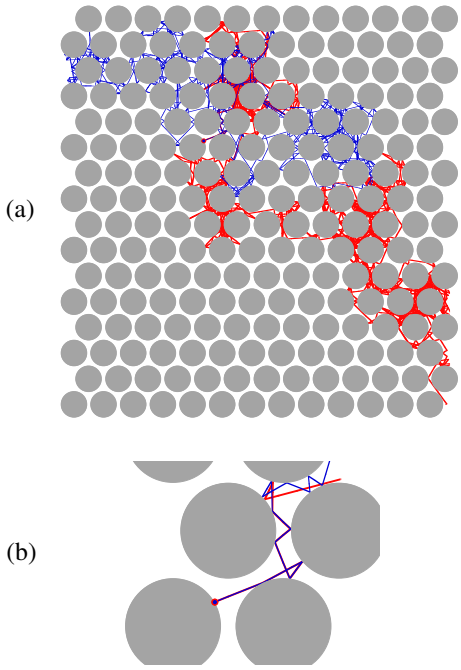


FIG. 9: Two trajectories of the periodic hard-disk Lorentz gas. They start from the same position but have velocities that differ by one part in a million. (a) Both trajectories depicted on large spatial scales. (b) Initial segments of both trajectories showing the sensitivity to initial conditions.

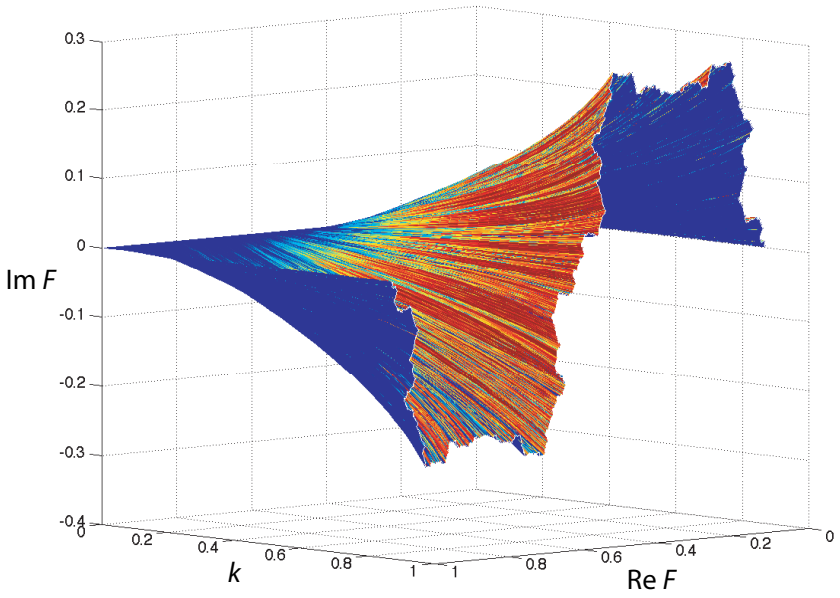


FIG. 10: The diffusive modes of the periodic hard-disk Lorentz gas represented by their cumulative function depicted in the complex plane $(\mathrm{Re}\, F_{\boldsymbol{k}}, \mathrm{Im}\, F_{\boldsymbol{k}})$ versus the wavenumber $\boldsymbol{k}$.

### E. Remarks

The hydrodynamic modes are rigorously constructed at the microscopic level of description in the phase space of the Hamiltonian dynamics by suitably weighting each trajectory in order to obtain eigenstates of the microscopic Liouvillian operator. Since these modes are exponentially decaying at positive times they break the time-reversal symmetry of Liouville's equation in complete compatibility with the fundamental microscopic Hamiltonian dynamics.

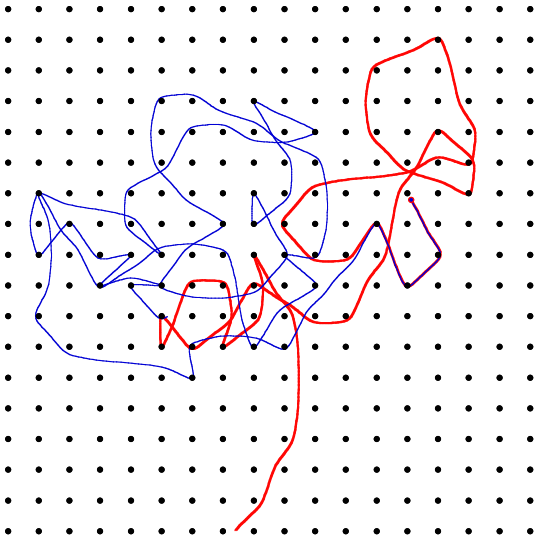

FIG. 11: Two trajectories of the periodic Yukawa-potential Lorentz gas. They start from the same position but have velocities that differ by one part in a million.

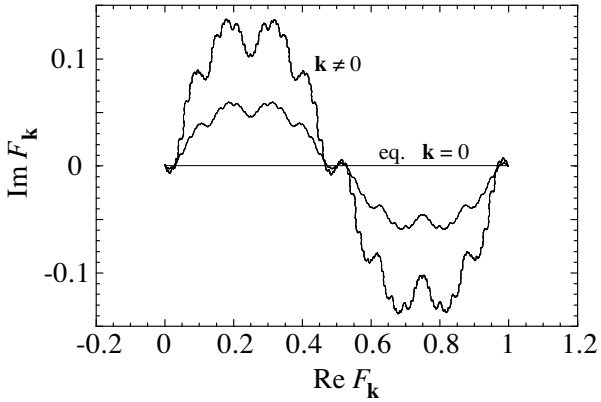


FIG. 12: The diffusive modes of the periodic Yukawa-potential Lorentz gas represented by their cumulative function depicted in the complex plane $(\mathrm{Re}\, F_{\boldsymbol{k}}, \mathrm{Im}\, F_{\boldsymbol{k}})$ for two different nonvanishing wavenumbers $\boldsymbol{k}$. The horizontal straight line is the curve corresponding to the vanishing wavenumber $\boldsymbol{k} = 0$ at which the mode reduces to the invariant microcanonical equilibrium state.

Time-reversal symmetry continues to be satisfied in the sense that the backward semigroup holds for negative times while the forward semigroup holds for positive times. Liouville's theorem is also satisfied which allows us to give a physical meaning to the probability distribution and to define a corresponding entropy. The transport coefficients are exactly defined so that the characteristic times of relaxation are well defined thanks to the spontaneous breaking of the time-reversal symmetry.

## VI. *AB INITIO* DERIVATION OF ENTROPY PRODUCTION

The singular character of the diffusive modes allows their exponential relaxation at the rate given by the dispersion relation of diffusion. Their explicit construction can be used to perform an *ab initio* derivation of entropy production directly from the microscopic Hamiltonian dynamics [8, 9].

The phase-space region $\mathcal{M}_{\boldsymbol{l}}$ corresponding to the lattice vector $\boldsymbol{l}$ is partitioned into cells $\mathcal{A}$. The probability that the system is found in the cell $\mathcal{A}$ at time $t$ is given by

$$P_t(\mathcal{A}) = \int_{\mathcal{A}} p_t(\boldsymbol{\Gamma})\, d\boldsymbol{\Gamma} \tag{75}$$

in terms of the probability density $p_t(\boldsymbol{\Gamma})$ which evolves in time according to Liouville's equation. The knowledge of the Pollicott-Ruelle resonances $s_j$ of the forward semigroup allows us to specify the approach to the equilibrium state as $t \to +\infty$:

$$P_t(\mathcal{A}) = P_{\rm eq}(\mathcal{A}) + \sum_j C_j \exp(s_j t) + \cdots \tag{76}$$

where the coefficients $C_j$ are calculated using the eigenstates associated with the resonances.

The coarse-grained entropy is defined in terms of these probabilities as

$$S_t(\mathcal{M}_l|\{\mathcal{A}\}) = -k_{\rm B} \sum_{\mathcal{A}} P_t(\mathcal{A}) \ln P_t(\mathcal{A}) \tag{77}$$

where $k_{\rm B}$ is Boltzmann's constant. As the consequence of Gibbs' mixing property and the decomposition (76), the coarse-grained entropy converges toward its equilibrium value $S_{\rm eq}$ at long times. We notice that the rates of convergence are given by the Pollicott-Ruelle resonances and are thus intrinsic to the system. At long times, the phase-space probability density becomes more and more inhomogeneous and acquires the singular character of the diffusive modes that control the long-time evolution. Therefore, the approach of the entropy toward its equilibrium value is determined by the diffusion coefficient. The time variation of the coarse-grained entropy over a time interval $\tau$

$$\Delta^\tau S = S_t(\mathcal{M}_{\boldsymbol{l}}|\{\mathcal{A}\}) - S_{t-\tau}(\mathcal{M}_{\boldsymbol{l}}|\{\mathcal{A}\}) \tag{78}$$

can be separated into the *entropy flow*

$$\Delta^\tau_{\rm e} S \equiv S_{t-\tau}(\boldsymbol{\Phi}^{-\tau}\mathcal{M}_{\boldsymbol{l}}|\{\mathcal{A}\}) - S_{t-\tau}(\mathcal{M}_{\boldsymbol{l}}|\{\mathcal{A}\}) \tag{79}$$

and the *entropy production*

$$\Delta^\tau_{\rm i} S \equiv \Delta^\tau S - \Delta^\tau_{\rm e} S = S_t(\mathcal{M}_{\boldsymbol{l}}|\{\mathcal{A}\}) - S_t(\mathcal{M}_{\boldsymbol{l}}|\{\boldsymbol{\Phi}^\tau\mathcal{A}\}) \tag{80}$$

This latter can be calculated using the construction of the diffusive modes described here above, as shown elsewhere [1, 8, 9]. Finally, we obtain the fundamental result that the entropy production takes the value expected from nonequilibrium thermodynamics

$$\Delta^\tau_{\rm i} S \simeq \tau\, k_{\rm B}\, \mathcal{D}\, \frac{(\nabla n)^2}{n} \tag{81}$$

where $n = P_t(\mathcal{M}_l)$ is the particle density [8, 9]. Remarkably, this result holds for partitions into arbitrarily fine cells and is therefore a general result independent of the particular coarse graining which is adopted. This result is a consequence of the singular character of the diffusive modes defined as Liouvillian eigenstates. It can indeed be shown that the entropy production would vanish if these modes had a density given by a function instead of a singular distribution [1, 8, 9]. This result shows that the singular character of the nonequilibrium states plays a fundamental role in giving a positive entropy production. The thermodynamic value of the entropy production is thus coming from the microscopic Hamiltonian dynamics itself.

## VII. ESCAPE-RATE THEORY

The spontaneous breaking of time-reversal symmetry also manifests itself in the escape-rate theory, which consists in putting the system out of equilibrium by allowing the escape of trajectories from some phase-space region [1, 37–40]. If this region is adequately chosen the escape rate can be directly related to a transport coefficient. This escape rate is the leading Pollicott-Ruelle resonance of the dynamics in such open systems. Dynamical systems theory has shown that this escape rate is given by the difference between the sum of positive Lyapunov exponents and the Kolmogorov-Sinai entropy per unit time [14]. Accordingly, the escape-rate theory allows us to establish relationships between the transport coefficients and the characteristic quantities of the microscopic dynamics.

### A. Helfand moments and transport coefficients

It is well known that each transport coefficients is given by a Green-Kubo formula or, equivalently, by an Einstein formula:

$$\alpha = \int_0^\infty \langle j_\alpha(t) j_\alpha(0)\rangle\, dt = \lim_{t\to\infty} \frac{1}{2t}\, \langle (G_\alpha(t) - G_\alpha(0))^2\rangle \tag{82}$$

TABLE III: Helfand moments of different transport properties. $V$ is the volume of the system and $T$ the temperature. The particles have positions $\boldsymbol{r}_a = (x_a, y_a, z_a)$, momenta $\boldsymbol{p}_a = (p_{ax}, p_{ay}, p_{az})$ $(a = 1, 2, ..., N)$, energy $E_a = \frac{\boldsymbol{p}_a^2}{2m} + \frac{1}{2}\sum_{b(\neq a)} u(r_{ab})$, and electric charge $eZ_a$. $N^{(\mathrm{r})}$ is the number of reactive events during a chemical reaction.

| irreversible property ($\alpha$) | Helfand moment $G_\alpha$ |
|---|---|
| shear viscosity ($\eta$) | $\frac{1}{\sqrt{V k_\mathrm{B} T}} \sum_{a=1}^{N} x_a \, p_{ay}$ |
| other viscosity ($\psi = \zeta + \frac{4}{3}\eta$) | $\frac{1}{\sqrt{V k_\mathrm{B} T}} \sum_{a=1}^{N} x_a \, p_{ax}$ |
| heat conduction ($\kappa$) | $\frac{1}{\sqrt{V k_\mathrm{B} T^2}} \sum_{a=1}^{N} x_a \, (E_a - \langle E_a \rangle)$ |
| electric conductivity ($\sigma$) | $\frac{1}{\sqrt{V k_\mathrm{B} T}} \sum_{a=1}^{N} eZ_a \, x_a$ |
| diffusion ($\mathcal{D}$) | $x_a$ |
| reaction ($L$) | $\frac{1}{\sqrt{V}} \, (N^{(\mathrm{r})} - \langle N^{(\mathrm{r})} \rangle)$ |

in terms of the Helfand moment defined as the time integral of the current [41]:

$$G_\alpha(t) = G_\alpha(0) + \int_0^t j_\alpha(t') \, dt' \tag{83}$$

The Helfand moment is the center of mass, energy or momentum of the moving particles, depending on whether the transport property is diffusion, heat conductivity, or viscosity. The Helfand moments associated with the different transport properties are given in Table III. Einstein formula shows that the Helfand moment undergoes a diffusive random walk, which suggests to set up a first-passage problem beyond a certain threshold for the Helfand moment. This threshold corresponds to the boundary of some region in the phase space of all the particles. Most of the trajectories escape from this phase-space region, but there might exist a zero-probability set of trajectories remaining inside this region. Typically, this set is a fractal composed of unstable trajectories.

The diffusive random walk of the Helfand moment is ruled by a diffusion equation. If the phase-space region is defined by requiring $|G_\alpha(t)| < \chi/2$, the escape rate can be computed as the leading eigenvalue of the diffusion equation with these absorbing boundary conditions for the Helfand moment [37, 39]:

$$\gamma \simeq \alpha \left(\frac{\pi}{\chi}\right)^2 \qquad \text{for} \quad \chi \to \infty \tag{84}$$

hence the proportionality between the escape rate $\gamma$ and the transport coefficient $\alpha$.

### B. Escape-rate formula in dynamical systems theory

A natural invariant probability measure can be constructed on the set of trajectories which are remaining in the phase-space region delimited by the threshold on the Helfand moment. It is invariant under the microscopic Hamiltonian dynamics. This invariant probability measure can be built from the eigenstate of the Liouvillian operator associated with the escape rate, which is the leading Pollicott-Ruelle resonance. The phase-space region is partitioned into cells labeled by $\omega$. The trajectories visiting the sequence of cells $\boldsymbol{\omega} = \omega_0\omega_1\omega_2...\omega_{n-1}$ at the successive times $t = 0, \tau, 2\tau, ..., (n-1)\tau$ form a path or history. A perturbation on the trajectories of this path is amplified by the stretching factor $\Lambda(\boldsymbol{\omega}) = \Lambda(\omega_0\omega_1\omega_2...\omega_{n-1})$. The sum of positive Lyapunov exponents of these trajectories is then

given by

$$\sum_{\lambda_i>0} \lambda_i = \lim_{n\to\infty} \frac{1}{n\tau} \ln |\Lambda(\omega_0\omega_1\omega_2...\omega_{n-1})| \tag{85}$$

The classical mechanics is naturally weighting the paths according to their instability. The higher the instability the smaller the probability weight according to

$$P(\boldsymbol{\omega}) = \frac{|\Lambda(\boldsymbol{\omega})|^{-1}}{\sum_{\boldsymbol{\omega}} |\Lambda(\boldsymbol{\omega})|^{-1}} \tag{86}$$

in the limit $n \to \infty$ [1]. This probability is normalized to unity by the denominator which decays at the escape rate:

$$\gamma = \lim_{n\tau\to\infty} -\frac{1}{n\tau} \ln \sum_{\boldsymbol{\omega}} \frac{1}{|\Lambda(\boldsymbol{\omega})|} \tag{87}$$

so that

$$\frac{P(\boldsymbol{\omega})}{|\Lambda(\boldsymbol{\omega})|^{-1}} \sim \exp(\gamma t) \tag{88}$$

On the other hand, the dynamical randomness is characterized by the Kolmogorov-Sinai entropy per unit time

$$h_{\rm KS} = {\rm Sup}_{\mathcal{P}} \lim_{n\to\infty} -\frac{1}{n\tau} \sum_{\boldsymbol{\omega}} P(\boldsymbol{\omega}) \ln P(\boldsymbol{\omega}) \tag{89}$$

where the supremum is taken over all the possible partitions $\mathcal{P}$ of the phase-space region containing the non-escaping trajectories into cells $\omega$ [1, 14]. The Kolmogorov-Sinai entropy is the mean decay rate of the probability (86):

$$P(\boldsymbol{\omega}) \sim \exp(-h_{\rm KS}\, t) \tag{90}$$

A similar relation holds for the stretching factors:

$$|\Lambda(\boldsymbol{\omega})| \sim \exp\left(\sum_{\lambda_i>0} \lambda_i\, t\right) \tag{91}$$

Introducing these relations in Eq. (88) for the invariant probability, we obtain the escape-rate formula

$$\gamma = \sum_{\lambda_i>0} \lambda_i - h_{\rm KS} \tag{92}$$

according to which the escape rate is the difference between the sum of positive Lyapunov exponents and the Kolmogorov-Sinai entropy per unit time [1, 14]. In a closed system without escape, the escape rate vanishes $\gamma = 0$, and we recover Pesin relation $h_{\rm KS} = \sum_{\lambda_i>0} \lambda_i$ showing that dynamical randomness finds its origin in the sensitivity to initial conditions [16]. However, in nonequilibrium systems with escape, there is a disbalance between dynamical randomness and the dynamical instability due to the escape of trajectories as schematically depicted in Fig. 13. Out of equilibrium, the system has less dynamical randomness than possible by the dynamical instability.

In systems with two degrees of freedom such as the two-dimensional Lorentz gases, there is a single positive Lyapunov exponent $\lambda$ and the partial Hausdorff dimension of the set of non-escaping trajectories can be estimated by the ratio of the Kolmogorov-Sinai entropy to the Lyapunov exponent [1, 38]

$$d_{\rm H} \simeq \frac{h_{\rm KS}}{\lambda} \tag{93}$$

so that the escape rate can be directly related to the fractal dimension and the Lyapunov exponent

$$\gamma \simeq \lambda(1 - d_{\rm H}) \tag{94}$$

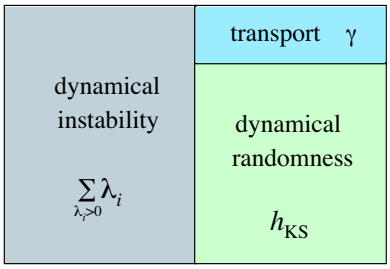


FIG. 13: Diagram showing how dynamical instability characterized by the sum of positive Lyapunov exponents $\sum_{\lambda_i>0} \lambda_i$ contributes to dynamical randomness characterized by the Kolmogorov-Sinai entropy per unit time $h_{\rm KS}$ and to the escape $\gamma$ due to transport according to the chaos-transport formula (95).

### C. The chaos-transport formula

If we combine the escape-rate formula (92) with the result (84) that the escape rate is proportional to the transport coefficient, we obtain the following large-deviation relationships between the transport coefficients and the characteristic quantities of chaos [37, 39]

$$\alpha \;=\; \lim_{\chi,V\to\infty} \left(\frac{\chi}{\pi}\right)^2 \left(\sum_{\lambda_i>0} \lambda_i - h_{\rm KS}\right)_\chi \tag{95}$$

This formula has already been applied to diffusion in periodic and random Lorentz gases [38, 42], reaction-diffusion [34], and viscosity [43, 44].

For diffusion in the open two-dimensional periodic Lorentz gas with parallel absorbing walls separated by the distance $L$, Eq. (95) shows that the diffusion coefficient is given by [38]

$$\mathcal{D} \;=\; \lim_{L\to\infty} \left(\frac{L}{\pi}\right)^2 \lambda\ (1-d_{\rm H})\Big|_L \tag{96}$$

which is a formula similar to Eq. (66) given that the wavenumber is here equal to $k=\pi/L$. A difference is that the Hausdorff dimension of the fractal curves in the complex plane are larger than unity while the partial Hausdorff dimension of the non-escaping trajectories is smaller than unity. These chaos-transport formulas apply to Hamiltonian systems satisfying Liouville's theorem.

## VIII. TIME ASYMMETRY IN DYNAMICAL RANDOMNESS

### A. Randomness of fluctuations in nonequilibrium steady states

In this section, we consider a system in a nonequilibrium steady state, such as a conductor between two particle reservoirs at different chemical potentials (see Fig. 14). The state $\omega$ of the system at a given time can be represented by the numbers $\{N_i\}_{i=1}^L$ of particles in the different cells $\{\mathrm{X}_i\}_{i=1}^L$ composing the conductor [2]. These numbers randomly change with time according to the motion of the particles along the conductor. In a nonequilibrium steady state, the conductor is crossed by a mean current from the reservoir at the highest chemical potential to the other one. The path of the system is the sequence of states $\boldsymbol{\omega} = \omega_0\omega_1\omega_2...\omega_{n-1}$ at the successive times $t = 0, \tau, 2\tau, ..., (n-1)\tau$. In a stationary state, a probability $P(\boldsymbol{\omega}) = P(\omega_0\omega_1\omega_2...\omega_{n-1})$ is assigned to each path. This invariant probability distribution describes the fluctuations in the numbers of particles in the cells of the conductor. In a nonequilibrium steady state, we should expect that the particles enter into the conductor at the two concentrations fixed by the chemical potentials of both reservoirs. However, they exit the conductor from either the left- or the right-hand side after having been mixed by the dynamics internal to the conductor, so that the outgoing particles are statistically correlated on fine phase-space scales. Reversing the time would require that the particles are injected with these

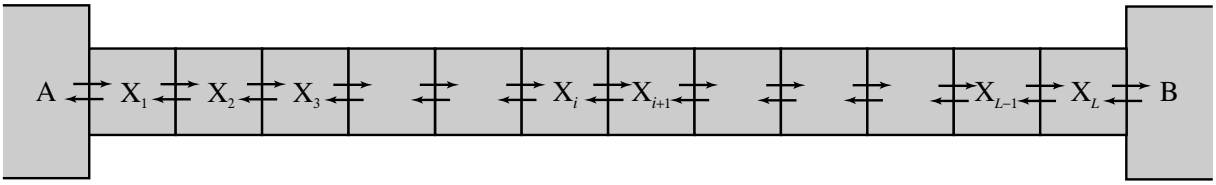


FIG. 14: Schematic representation of the diffusion process of particles in a conductor composed of $L$ cells $\{\mathrm{X}_i\}_{i=1}^{L}$ of volume $\Delta V$ between two particle reservoirs, A and B.

fine statistical correlations in order that they exit unmixed at both reservoirs. Although the time-reversal steady state is possible, it is highly improbable and clearly distinct from the actual steady state. This reasoning shows that the probability of a typical path $\boldsymbol{\omega} = \omega_0\omega_1\omega_2...\omega_{n-1}$ should be different from the probability of its time reversal $\boldsymbol{\Theta}(\boldsymbol{\omega}) = \boldsymbol{\omega}^{\mathrm{R}} = \omega_{n-1}...\omega_2\omega_1\omega_0$. This is possible because the trajectories of typical paths are distinct from their time reversal as pointed out in Section III. The nonequilibrium boundary conditions explicitly break the time-reversal symmetry.

The dynamical randomness of the nonequilibrium process can be characterized by the decay of the path probabilities as defined by the entropy per unit time [12–14]

$$h \equiv \lim_{n\to\infty} -\frac{1}{n\tau}\sum_{\boldsymbol{\omega}} P(\boldsymbol{\omega})\ln P(\boldsymbol{\omega}) = \lim_{n\to\infty} -\frac{1}{n\tau}\sum_{\omega_0\omega_1\omega_2...\omega_{n-1}} P(\omega_0\omega_1\omega_2...\omega_{n-1})\ln P(\omega_0\omega_1\omega_2...\omega_{n-1}) \tag{97}$$

The Kolmogorov-Sinai entropy per unit time is defined in Eq. (89) as the supremum of $h$ over all the possible partitions $\mathcal{P}$. Since we expect that the probability of the nonequilibrium steady state is not time-reversal symmetric, the probability of the time-reversed paths should decay at a different rate, which can be called a time-reversed entropy per unit time [3]

$$h^{\mathrm{R}} \equiv \lim_{n\to\infty} -\frac{1}{n\tau}\sum_{\boldsymbol{\omega}} P(\boldsymbol{\omega})\ln P(\boldsymbol{\omega}^{\mathrm{R}}) = \lim_{n\to\infty} -\frac{1}{n\tau}\sum_{\omega_0\omega_1\omega_2...\omega_{n-1}} P(\omega_0\omega_1\omega_2...\omega_{n-1})\ln P(\omega_{n-1}...\omega_2\omega_1\omega_0) \tag{98}$$

For almost all paths with respect to the probability measure $P$, we would have

$$P(\boldsymbol{\omega}) = P(\omega_0\omega_1\omega_2...\omega_{n-1}) \;\sim\; \exp(-hn\tau) \tag{99}$$

$$P(\boldsymbol{\omega}^{\mathrm{R}}) = P(\omega_{n-1}...\omega_2\omega_1\omega_0) \;\sim\; \exp(-h^{\mathrm{R}}n\tau) \tag{100}$$

The first line is known as the Shannon-McMillan-Breiman theorem [1], the second is its extension for stationary states which are not time-reversal symmetric. The entropy per unit time $h$ characterizes the dynamical randomness of the process. The faster the decay of the path probabilities, the larger the proliferation of these paths as time increases. Therefore, the larger the entropy per unit time $h$, the higher the temporal disorder of the time evolution. The time-reversed entropy per unit time $h^{\mathrm{R}}$ characterizes the decay of the time reversals of the typical paths in a similar way and it thus characterizes the dynamical randomness of the backward paths.

### B. Entropy production

The most remarkable result is that the difference between both entropies per unit time (98) and (97) gives the entropy production of the nonequilibrium steady state:

$$\frac{1}{k_{\mathrm{B}}}\frac{d_{\mathrm{i}}S}{dt} = h^{\mathrm{R}} - h \geq 0 \tag{101}$$

in the limit $\tau \to 0$ [3]. An equivalent statement is that the ratio of the probabilities (99) and (100) grows as the entropy production

$$\frac{P(\boldsymbol{\omega})}{P(\boldsymbol{\omega}^{\mathrm{R}})} = \frac{P(\omega_0\omega_1\omega_2...\omega_{n-1})}{P(\omega_{n-1}...\omega_2\omega_1\omega_0)} \sim \exp\left[n\tau(h^{\mathrm{R}} - h)\right] = \exp\left(\frac{n\tau}{k_{\mathrm{B}}}\frac{d_{\mathrm{i}}S}{dt}\right) \tag{102}$$

For an isothermal process, the logarithm of the ratio of the probabilities thus gives the work dissipated along the path:

$$\ln\frac{P(\boldsymbol{\omega})}{P(\boldsymbol{\omega}^{\mathrm{R}})} \simeq \frac{\mathcal{W}_{\mathrm{diss}}(\boldsymbol{\omega})}{k_{\mathrm{B}}T} \tag{103}$$

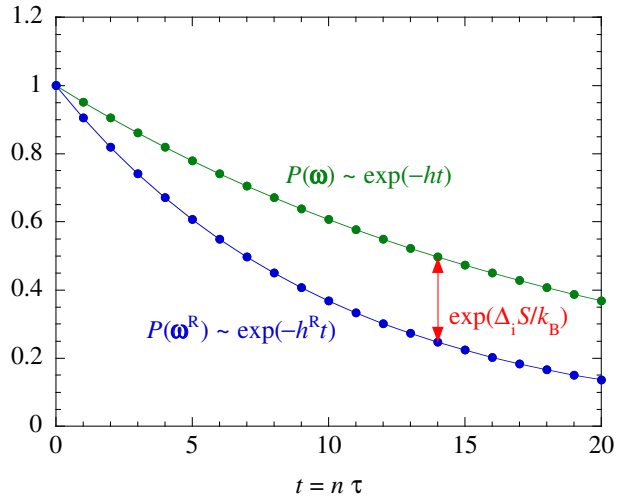


FIG. 15: Diagram showing the probability of a path and the probability of the corresponding time reversal as a function of the number $n$ of time intervals $\tau$, illustrating the formula (101). $\Delta_{\mathrm{i}}S$ denotes the entropy production during the whole duration $n\tau$.

as $n \to \infty$ while $\tau \to 0$.

The formula (101) gives a non-negative entropy production in agreement with the second law of thermodynamics. Indeed, the non-negativity of the right-hand member is guaranteed by the fact that the difference between Eqs. (98) and (97) is a relative entropy that is known to be non-negative:

$$\frac{1}{k_{\mathrm{B}}}\frac{d_{\mathrm{i}}S}{dt} = \lim_{n\to\infty}\frac{1}{n\tau}\sum_{\boldsymbol{\omega}} P(\boldsymbol{\omega}) \ln\frac{P(\boldsymbol{\omega})}{P(\boldsymbol{\omega}^{\mathrm{R}})} \geq 0 \tag{104}$$

Consequently, we have the general property that

$$h^{\mathrm{R}} \geq h \tag{105}$$

The equality $h^{\mathrm{R}} = h$ holds if and only if the probabilities of the paths are equal to the probabilities of their time reversals:

$$P(\boldsymbol{\omega}) = P(\boldsymbol{\omega}^{\mathrm{R}}) \qquad \text{for all} \quad \boldsymbol{\omega} \tag{106}$$

This is the condition of detailed balance which holds in the equilibrium state where entropy production vanishes.

The property (105) means that, in a nonequilibrium steady state, the probabilities of the typical paths decay more slowly than the probabilities of their time reversals (see Fig. 15). In this sense, the temporal disorder is smaller for typical paths than for their time reversal. We thus have the following

**Principle of temporal ordering:** *In nonequilibrium steady states, the typical paths are more ordered in time than their corresponding time reversals.*

This principle and the formula (101) show that entropy production results from a time asymmetry in the dynamical randomness in nonequilibrium steady states. It is remarkable that this ordering phenomenon appears if we consider the evolution of the process as a movie, looking for regularities in the sequence of pictures. The temporal ordering is compatible with Boltzmann's interpretation of the second law according to which spatial disorder increases with time. In a sense, the temporal ordering is possible at the expense of spatial disorder.

We notice the similarity of the structures of Eq. (101) with the chaos-transport relationship (95). Indeed, both formulas are large-deviation dynamical relationships giving an irreversible property from the difference between two quantities characterizing the dynamical randomness or instability of the microscopic dynamics (see Fig. 16).

Formula (101) can be proved in different contexts.

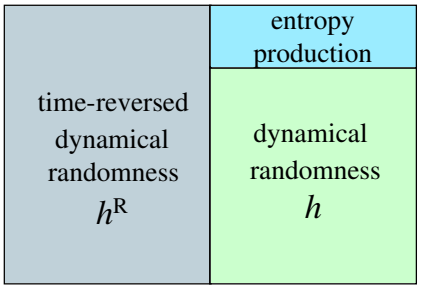


FIG. 16: Diagram showing how the dynamical randomness of the backward paths characterized by the time-reversed entropy per unit time $h^{\mathrm{R}}$ contributes to dynamical randomness characterized by the entropy per unit time $h$ and to the entropy production $(1/k_{\mathrm{B}})d_{\mathrm{i}}S/dt$ according to the formula (101). We notice the similarity of the structure with Fig. 13.

### 1. *Proof for continuous-time jump processes*

These stochastic processes are ruled by master equations of Pauli type:

$$\frac{d}{dt}P_t(\omega) = \sum_{\rho,\omega'(\neq\omega)} [P_t(\omega')W_\rho(\omega'|\omega) - P_t(\omega)W_{-\rho}(\omega|\omega')] \tag{107}$$

for the probability $P_t(\omega)$ to find the system in the state $\omega$ by the time $t$ [5]. $W_\rho(\omega|\omega')$ denotes the rate of the transition $\omega \to \omega'$ for the elementary process $\rho$. A transition rate is associated with several possible elementary processes $\rho = \pm 1, \pm 2, ..., \pm r$. The probabilities are constant in a steady state: $dP(\omega)/dt = 0$.

The dynamical randomness of such stochastic processes can be characterized by the $\tau$-entropy per unit time introduced more than ten years ago [45]

$$h(\tau) = \left(\ln \frac{\mathrm{e}}{\tau}\right) \sum_{\rho,\omega,\omega'} P(\omega)\ W_\rho(\omega|\omega') - \sum_{\rho,\omega,\omega'} P(\omega)\ W_\rho(\omega|\omega')\ \ln W_\rho(\omega|\omega') + O(\tau) \tag{108}$$

and the time-reversed $\tau$-entropy per unit time [3]

$$h^{\mathrm{R}}(\tau) = \left(\ln \frac{\mathrm{e}}{\tau}\right) \sum_{\rho,\omega,\omega'} P(\omega)\ W_\rho(\omega|\omega') - \sum_{\rho,\omega,\omega'} P(\omega)\ W_\rho(\omega|\omega')\ \ln W_{-\rho}(\omega'|\omega) + O(\tau) \tag{109}$$

We notice that the expressions (108) and (109) differ by the transition rate in the logarithm. Their difference is equal to the known expression for the entropy production of these stochastic processes [46, 47]

$$h^{\mathrm{R}}(\tau) - h(\tau) = \frac{1}{2} \sum_{\rho,\omega,\omega'} [P(\omega)\ W_\rho(\omega|\omega') - P(\omega')\ W_{-\rho}(\omega'|\omega)]\ \ln \frac{P(\omega)\ W_\rho(\omega|\omega')}{P(\omega')\ W_{-\rho}(\omega'|\omega)} + O(\tau) \simeq \frac{1}{k_{\mathrm{B}}} \frac{d_{\mathrm{i}}S}{dt} \tag{110}$$

in the limit $\tau \to 0$. This proves the relationship (101) [3].

### 2. *Proof for thermostated dynamical systems*

Thermostated dynamical systems are deterministic systems with non-Hamiltonian forces modeling the dissipation of energy toward a thermostat [48]. The non-Hamiltonian forces are chosen in such a way that the equations of motion are time-reversal symmetric. In these systems, the stochastic fluctuations of the reaction of the thermostat back onto the system are neglected. The nonequilibrium steady states are described by SRB invariant probability measures which spontaneously break the time-reversal symmetry.

The phase space is partitioned into cells $\omega$ of diameter $\delta$. In the limit of an arbitrarily fine partition, the entropy per unit time tends to the Kolmogorov-Sinai entropy per unit time which is equal to the sum of positive Lyapunov exponents by Pesin theorem [16]:

$$\lim_{\delta \to 0} h = \sum_{\lambda_i > 0} \lambda_i = h_{\mathrm{KS}} \tag{111}$$

In the same limit, the time-reversed entropy per unit time is equal to minus the sum of negative Lyapunov exponents:

$$\lim_{\delta\to 0} h^{\mathrm{R}} = -\sum_{\lambda_i<0} \lambda_i \tag{112}$$

The difference between both entropies per unit time is minus the sum of all the Lyapunov exponents which is the rate of contraction of the phase-space volumes under the effects of the non-Hamiltonian forces:

$$\lim_{\delta\to 0} \left(h^{\mathrm{R}} - h\right) = -\sum_{i} \lambda_i = \frac{1}{k_{\mathrm{B}}} \frac{d_{\mathrm{i}} S}{dt} \tag{113}$$

This contraction rate has been identified in these models as the rate of entropy production [49], which proves the formula (101) in this case as well.

### *3. Proof with the escape-rate theory*

The formula (101) can also be proved with the escape-rate theory. We consider the escape of particles by difffusion from a large reservoir, as depicted in Fig. 17. The density of particles is uniform inside the reservoir and linear in the slab where diffusion takes place. The density decreases from the uniform value $N/V$ of the reservoir down to zero at the exit where the particles escape. The width of the diffusive slab is equal to $L$ so that the gradient is given by $\nabla n = -N/(VL)$ and the particle current density $J = -\mathcal{D}\nabla n = \mathcal{D}N/(VL)$. Accordingly, the number of particles in the reservoir decreases at the rate

$$\frac{dN}{dt} = -\int \boldsymbol{J}\cdot d\boldsymbol{\Sigma} = \int \mathcal{D}\,\boldsymbol{\nabla} n \cdot d\boldsymbol{\Sigma} = -\mathcal{D}\,\frac{A}{VL} N \tag{114}$$

Therefore, the number of particles decreases exponentially as

$$N(t) = N(0)\,\exp(-\gamma t) \tag{115}$$

at the escape rate

$$\gamma = \mathcal{D}\,\frac{A}{VL} \tag{116}$$

In the limit of an arbitrarily large reservoir $N, V \to \infty$ with $n = N/V$ constant, the escape rate vanishes and a nonequilibrium steady state establishes itself in the diffusive slab.

The entropy production can be calculated by using the thermodynamic expression (81) as

$$\frac{1}{k_{\mathrm{B}}}\frac{d_{\mathrm{i}} S}{dt} = \int \mathcal{D}\,\frac{(\nabla n)^2}{n}\,d^3r = \mathcal{D}\,\frac{A}{VL} N = \gamma N \tag{117}$$

which is proportional to the escape rate of individual particles.

According to dynamical systems theory, the escape rate is given by the difference (92) between the sum of positive Lyapunov exponents and the Kolmogorov-Sinai entropy . Since the dynamics is Hamiltonian and satisfies Liouville's theorem, the sum of positive Lyapunov exponents is equal to minus the sum of negative ones:

$$\gamma = \sum_{\lambda_i>0} \lambda_i - h_{\mathrm{KS}} = -\sum_{\lambda_i<0} \lambda_i - h_{\mathrm{KS}} \tag{118}$$

Now, the entropies per unit time in Eq. (101) concern the dynamics of the $N$ particles. Here, the particles are independent of each other so that the entropies per unit time of the $N$-particle system is equal to $N$ times the entropies per unit time of the one-particle system. On the other hand, we have seen with Eq. (112) that minus the sum of negative Lyapunov exponents should correspond to the time-reversed entropy per unit time so that we can here also prove Eq. (101):

$$\frac{1}{k_{\mathrm{B}}}\frac{d_{\mathrm{i}} S}{dt} = N\left(-\sum_{\lambda_i<0} \lambda_i - h_{\mathrm{KS}}\right)_1 = \left(h^{\mathrm{R}} - h\right)_N \tag{119}$$

in the infinite-reservoir limit $N, V \to \infty$ with $n = N/V$ constant with a nonequilibrium steady state in the diffusive slab.

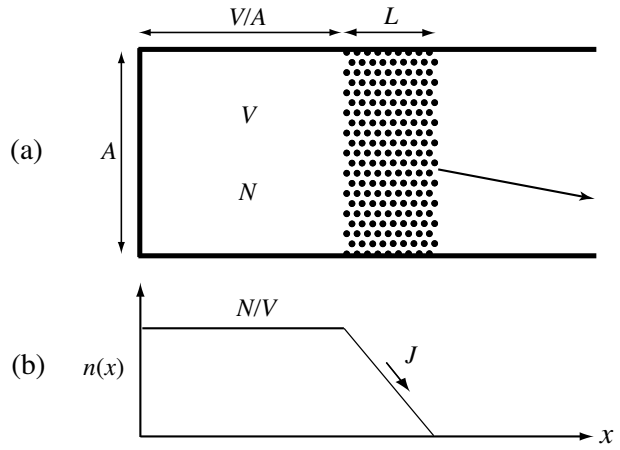


FIG. 17: (a) Escape of $N$ particles from a reservoir of volume $V$ and area $A$ by diffusion through a slab of width $L$ and area $A$. (b) The profile of concentration $n(x)$ which is uniform in the reservoir and linear in the diffusive slab.

### C. Markov chains and information theoretic aspects

The entropies per unit time as well as the thermodynamic entropy production entering in the formula (101) can be interpreted in terms of the numbers of paths satisfying different conditions. In this regard, important connections exist between information theory and the second law of thermodynamics.

In order to show these aspects, let us consider discrete-time Markov chains. The matrix of transition probabilities is denoted $P_{\omega\omega'}$, which is the conditional probability that the system is in the state $\omega'$ at time $n+1$ if it was in the state $\omega$ at time $n$. The time is counted in units of the time interval $\tau$. The matrix of transition probabilities satisfies

$$\sum_{\omega'} P_{\omega\omega'} = 1 \tag{120}$$

In a steady state, the probabilities $p_\omega$ to find the system in given states are obtained by solving the stationary equation

$$\sum_{\omega} p_\omega P_{\omega\omega'} = p_{\omega'} \tag{121}$$

The dynamical randomness of this Markov chain is characterized by the Kolmogorov-Sinai entropy per unit time

$$h = -\sum_{\omega,\omega'} p_\omega P_{\omega\omega'} \ln P_{\omega\omega'} \tag{122}$$

On the other hand, the time-reversed entropy per unit time is here given by

$$h^{\mathrm{R}} = -\sum_{\omega,\omega'} p_\omega P_{\omega\omega'} \ln P_{\omega'\omega} \tag{123}$$

We notice that the only difference between both dynamical entropies is the exchange of $\omega$ and $\omega'$ in the transition probabilities appearing in the logarithm. According to Eq. (101), the thermodynamic entropy production of this process would be equal to

$$\Delta_{\mathrm{i}} S = h^{\mathrm{R}} - h \tag{124}$$

in units of the time interval $\tau$ and Boltzmann's constant $k_{\mathrm{B}}$.

For Markov chains with two states $\{0,1\}$, it turns out that we always have the equality $h^{\mathrm{R}} = h$ so that they are not appropriate to model nonequilibrium processes.

Next, we can consider a Markov chain with three states $\{1,2,3\}$ with the following matrix of transition probabilities

$$\boldsymbol{P} = \begin{pmatrix} \frac{a}{2} & 1-a & \frac{a}{2} \\ \frac{a}{2} & \frac{a}{2} & 1-a \\ 1-a & \frac{a}{2} & \frac{a}{2} \end{pmatrix} \tag{125}$$

where $0 \leq a \leq 1$ is a parameter. The entropies per unit time of this Markov chain are given by

$$h = -a \ln \frac{a}{2} - (1-a) \ln(1-a) \tag{126}$$

$$h^{\mathrm{R}} = -\left(1 - \frac{a}{2}\right) \ln \frac{a}{2} - \frac{a}{2} \ln(1-a) \tag{127}$$

whereupon the entropy production is

$$\Delta_{\mathrm{i}} S = h^{\mathrm{R}} - h = \left(1 - \frac{3a}{2}\right) \ln \frac{2(1-a)}{a} \geq 0 \tag{128}$$

These quantities are depicted in Fig. 18. The entropy production vanishes at equilibrium $a = 2/3$ where $h = h^{\mathrm{R}} = \ln 3$. The entropy production is infinite and the process fully irreversible at $a = 1$ where $h = \ln 2$ and $a = 0$ where $h = 0$, in which case the process is perfectly cyclic ...123123123123...

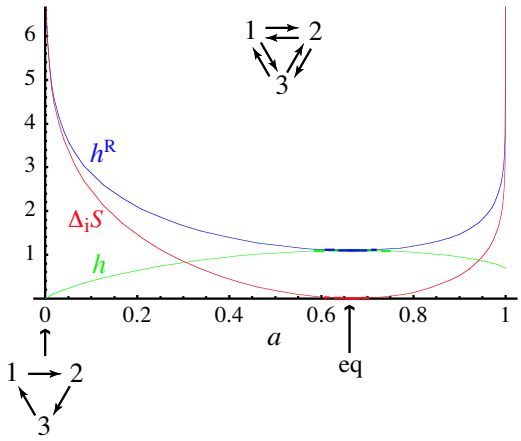


FIG. 18: The dynamical entropies (126) and (127) as well as the entropy production (128) for the three-state Markov chain defined by the matrix (125) of transition probabilities versus the parameter $a$. The equilibrium corresponds to the value $a = 2/3$. The process is perfectly cyclic at $a = 0$ where the path is ...123123123123... and the Kolmogorov-Sinai entropy $h$ vanishes as a consequence.

The number of typical paths generated by the random process increases as $\exp(h\,n)$. In this regard, the Kolmogorov-Sinai entropy per unit time is the rate of production of information by the random process. On the other hand, the time-reversed entropy per unit time is the rate of production of information by the time reversals of the typical paths. The thermodynamic entropy production is the difference between these two rates of information production. With the formula (101), we can recover a result by Landauer [50] and Bennett [51] that erasing information in the memory of a computer is an irreversible process of entropy production equal to $k_{\mathrm{B}} \ln 2$. Indeed, erasing the bits of a sequence of zeros and ones is a process without surprise so that its entropy per unit time vanishes $h = 0$. On the other hand, the time-reversed process lets the zeros and ones appear with surprises so that the time-reversed entropy per unit time is equal to $h^{\mathrm{R}} = \ln 2$. The difference between them gives the entropy production $\Delta_{\mathrm{i}} S = k_{\mathrm{B}}(h^{\mathrm{R}} - h) = k_{\mathrm{B}} \ln 2$ [3]. The above reasoning confirms the solution of the paradox of Maxwell's demon given by Landauer and Bennett [50, 51], according to whom this demon produces entropy while erasing information so that its behavior is in agreement with the second law of thermodynamics.

### D. Fluctuation theorem for the currents

Further large-deviation dynamical relationships are the so-called fluctuation theorems, which concern the probability than some observable such as the work performed on the system would take positive or negative values under the effect of the nonequilibrium fluctuations. Since the early work of the fluctuation theorem in the context of thermostated systems [52–54], stochastic [55–59] as well as Hamiltonian [60] versions have been derived. A fluctuation theorem has also been derived for nonequilibrium chemical reactions [62]. A closely related result is the nonequilibrium work theorem [61] which can also be derived from the microscopic Hamiltonian dynamics.

Beside the work performed on the system, interesting quantities are the currents crossing a system in a nonequilibrium steady state. Recently, we have been able to derive a fluctuation theorem for the currents in the framework of the

stochastic master equation using Schnakenberg graph analysis [63–66]. According to Schnakenberg [46], a graph can be associated with some stochastic process: The states of the process are the vertices of the graph and the transitions the bonds. This analysis is very useful because it allows us to identify the affinities – that is, the thermodynamic forces imposed on the system by the differences of temperature or chemical potentials between the external reservoirs of heat or molecules. These affinities are given for instance by free energy differences $A_\alpha = \Delta F_\alpha/T$ and are the causes of the currents crossing the system. At the microscopic level, these currents fluctuate and depend on the path followed by the system: $j_\alpha(t;\boldsymbol{\omega})$. These currents can be the electric current in a conductor, the number of molecules of some reactant consumed in a chemical reaction, the rotation velocity of a rotary molecular motor, or local currents in a fluid element, as listed in Table II. A system can sustain several independent currents. The mean current over a time interval $t$ is defined by

$$J_\alpha(\boldsymbol{\omega}) = \frac{1}{t}\int_0^t j_\alpha(t';\boldsymbol{\omega})\, dt' \tag{129}$$

which is a fluctuating variable. The currents are odd under time reversal:

$$J_\alpha(\boldsymbol{\omega}^{\rm R}) = -J_\alpha(\boldsymbol{\omega}) \tag{130}$$

In a nonequilibrium steady state, the entropy production is the sum of the affinities multiplied by the mean currents:

$$\frac{d_{\rm i}S}{dt}\Big|_{\rm neq} = \sum_\alpha A_\alpha \langle J_\alpha\rangle > 0 \tag{131}$$

At the mesoscopic level, the currents fluctuate and the previous result (102) suggests that

$$\frac{P(\boldsymbol{\omega})}{P(\boldsymbol{\omega}^{\rm R})} = \frac{P(\omega_0\omega_1\omega_2...\omega_{n-1})}{P(\omega_{n-1}...\omega_2\omega_1\omega_0)} \simeq \exp\left[\frac{t}{k_{\rm B}}\sum_\alpha A_\alpha J_\alpha(\boldsymbol{\omega})\right] \tag{132}$$

where $t = n\tau$. Using this assumption, a schematic proof for the fluctuation theorem follows:

$$\begin{aligned}
P\left(\{J_\alpha = \xi_\alpha\}\right) &\simeq \sum_{\boldsymbol{\omega}} P(\boldsymbol{\omega})\,\delta\left[J_\alpha(\boldsymbol{\omega}) - \xi_\alpha\right] && (133)\\
&= \sum_{\boldsymbol{\omega}} P(\boldsymbol{\omega}^{\rm R})\,\delta\left[J_\alpha(\boldsymbol{\omega}^{\rm R}) - \xi_\alpha\right] && (134)\\
&\simeq \sum_{\boldsymbol{\omega}} P(\boldsymbol{\omega})\,{\rm e}^{-\frac{t}{k_{\rm B}}\sum_\alpha A_\alpha J_\alpha(\boldsymbol{\omega})}\,\delta\left[-J_\alpha(\boldsymbol{\omega}) - \xi_\alpha\right] && (135)\\
&= {\rm e}^{\frac{t}{k_{\rm B}}\sum_\alpha A_\alpha\xi_\alpha}\sum_{\boldsymbol{\omega}} P(\boldsymbol{\omega})\,\delta\left[J_\alpha(\boldsymbol{\omega}) + \xi_\alpha\right] && (136)\\
&\simeq {\rm e}^{\frac{t}{k_{\rm B}}\sum_\alpha A_\alpha\xi_\alpha} P\left(\{J_\alpha = -\xi_\alpha\}\right) && (137)
\end{aligned}$$

where $\delta(\cdot)$ denotes the product of Dirac delta distributions over all the currents of interest in the system. The first line is the definition of the probability that each fluctuating current $J_\alpha$ takes the value $\xi_\alpha$. The second line is obtained because the sum over all the paths $\boldsymbol{\omega}$ is equivalent to the sum over all the time-reserved paths $\boldsymbol{\omega}^{\rm R}$. Now, the probability $P(\boldsymbol{\omega}^{\rm R})$ of the time-reversed paths can be expressed by using Eq. (132) and we can use the odd parity (130) of the currents. In the third line, the delta shows that each current $J_\alpha$ now takes the negative value $-\xi_\alpha$, so that the exponential can exit the sum after specifying these values and the result is obtained. This leads to the *fluctuation theorem for the currents*

$$\frac{P\left(\{J_\alpha = \xi_\alpha\}\right)}{P\left(\{J_\alpha = -\xi_\alpha\}\right)} \simeq \exp\left(\frac{t}{k_{\rm B}}\sum_\alpha A_\alpha\xi_\alpha\right) \tag{138}$$

for $t \to \infty$. The rigorous proof of this fluctuation theorem is given elsewhere [63–65].

Different expressions can be given to the fluctuation theorem. If we introduce the decay rates of the probabilities that the currents take some values as

$$P\left(\{J_\alpha = \xi_\alpha\}\right) \sim \exp\left[-H\left(\{\xi_\alpha\}\right)t\right] \tag{139}$$

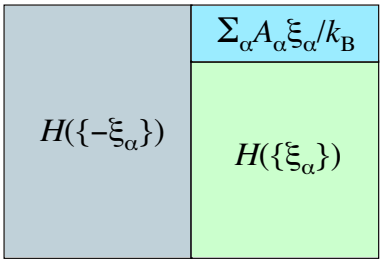


FIG. 19: Diagram illustrating the fluctuation theorem for the currents (140) showing how the decay rate at negative values of the currents equates the decay rate at positive value plus the irreversible value. Compare with Figs. 13 and 16.

the fluctuation theorem writes [64, 65]

$$H\left(\{-\xi_\alpha\}\right) - H\left(\{\xi_\alpha\}\right) = \frac{1}{k_B} \sum_\alpha A_\alpha \xi_\alpha \tag{140}$$

This form shows the deep similarity with the chaos-transport formula (95) and Eq. (101).

On the other hand, we can introduce the generating function of the mean currents and their statistical moments as

$$Q\left(\{\lambda_\alpha\}\right) = \lim_{t\to\infty} -\frac{1}{t} \ln \left\langle \exp\left[-\sum_\alpha \lambda_\alpha G_\alpha(t)\right]\right\rangle \tag{141}$$

with the Helfand moments $G_\alpha(t) = \int_0^t j_\alpha(t';\boldsymbol{\omega})dt' = t\, J_\alpha(\boldsymbol{\omega})$ associated with the fluctuating currents. This generating function is the Legendre transform of the decay function defined in Eq. (139). The fluctuation theorem for the currents is expressed in terms of this generating function as [63]

$$Q\left(\{A_\alpha - \lambda_\alpha\}\right) = Q\left(\{\lambda_\alpha\}\right) \tag{142}$$

We notice that the generating and decay functions characterize the nonequilibrium process in the steady state and, consequently, have a general dependence on the affinities which play the role of nonequilibrium parameters.

### E. Onsager reciprocity relations and generalizations to nonlinear response

In nonequilibrium steady states, the mean currents crossing the system depend on the nonequilibrium constraints given by the affinities or thermodynamic forces which vanish at equilibrium. Accordingly, the mean currents can be expanded in powers of the affinities around the equilibrium state. Many nonequilibrium processes are in the linear regime studied since Onsager classical work [7]. However, chemical reactions are known to involve the nonlinear regime. This is also the case for nanosystems such as the molecular motors as recently shown [66]. In the nonlinear regime, the mean currents depend on powers of the affinities so that it is necessary to consider the full Taylor expansion of the currents on the affinities:

$$\langle J_\alpha \rangle = \sum_\beta L_{\alpha\beta}\, A_\beta + \frac{1}{2}\sum_{\beta,\gamma} M_{\alpha\beta\gamma}\, A_\beta\, A_\gamma + \frac{1}{6}\sum_{\beta,\gamma,\delta} N_{\alpha\beta\gamma\delta}\, A_\beta\, A_\gamma\, A_\delta + \cdots \tag{143}$$

The coefficients $L_{\alpha\beta}$ are Onsager's linear-response coefficients. The other coefficients $M_{\alpha\beta\gamma}$, $N_{\alpha\beta\gamma\delta}$, and so on, characterize the nonlinear response of the system.

A direct consequence of the fluctuation theorem for the currents (138) is that these coefficients obey remarkable relations [63–65], the first of which are Onsager reciprocity relations as well as the Green-Kubo and Einstein formulas for these coefficients:

$$L_{\alpha\beta} = L_{\beta\alpha} = \frac{1}{2}\int_{-\infty}^{+\infty} \langle [j_\alpha(t) - \langle j_\alpha\rangle]\,[j_\beta(0) - \langle j_\beta\rangle]\rangle_{\rm eq}\, dt = \lim_{t\to\infty} \frac{1}{2t} \langle \Delta G_\alpha(t) \Delta G_\beta(t)\rangle_{\rm eq} \tag{144}$$

with $\Delta G_\alpha = G_\alpha - \langle G_\alpha\rangle$. Next, the third-order response coefficients can be expressed as

$$M_{\alpha\beta\gamma} = \tilde{R}_{\alpha\beta,\gamma} + \tilde{R}_{\alpha\gamma,\beta} \tag{145}$$

in terms of the sensitivity of the linear-response coefficients to nonequilibrium perturbations:

$$\tilde{R}_{\alpha\beta,\gamma} \equiv \frac{\partial}{\partial A_\gamma} \lim_{t\to\infty} \frac{1}{2t} \langle \Delta G_\alpha(t) \Delta G_\beta(t) \rangle_{\rm neq} \Big|_{\{A_\epsilon = 0\}} \tag{146}$$

Furthermore, the fourth-order response coefficients are given by

$$N_{\alpha\beta\gamma\delta} = \tilde{T}_{\alpha\beta,\gamma\delta} + \tilde{T}_{\alpha\gamma,\beta\delta} + \tilde{T}_{\alpha\delta,\beta\gamma} - \tilde{S}_{\alpha\beta\gamma,\delta} \tag{147}$$

in terms of

$$\tilde{T}_{\alpha\beta,\gamma\delta} = \frac{\partial}{\partial A_\gamma} \frac{\partial}{\partial A_\delta} \lim_{t\to\infty} \frac{1}{2t} \langle \Delta G_\alpha(t) \Delta G_\beta(t) \rangle_{\rm neq} \Big|_{\{A_\epsilon = 0\}} \tag{148}$$

which are similar to the coefficients (146), and

$$\tilde{S}_{\alpha\beta\gamma,\delta} = \frac{\partial}{\partial A_\delta} \lim_{t\to\infty} \frac{1}{2t} \langle \Delta G_\alpha(t) \Delta G_\beta(t) \Delta G_\gamma(t) \rangle_{\rm neq} \Big|_{\{A_\epsilon = 0\}} \tag{149}$$

which can be proved to be totally symmetric under all the permutations of the four indices [64, 65]. Similar relations also hold at higher orders. These results show that the fluctuation theorem, which is a consequence of microreversibility, plays a central role in nonequilibrium statistical mechanics because previous results and generalizations can be deduced thereof.

## IX. CONCLUSIONS AND PERSPECTIVES

In this paper, we have described recent advances in nonequilibrium statistical mechanics and have shown that they constitute a breakthrough which opens very new perspectives in our understanding of nonequilibrium processes and the second law of thermodynamics.

First of all, the time asymmetry of nonequilibrium processes finally finds an explanation at the microscopic level of description. It is nowadays possible to show that the modes of relaxation toward the equilibrium as well as the nonequilibrium steady states involve a spontaneous breaking of the time-reversal symmetry of the microscopic Hamiltonian dynamics at the level of the statistical description. Relaxation modes such as the diffusive modes can be constructed as eigenstates of the fundamental Liouvillian operator ruling the time evolution of the probability density in phase space. These eigenstates are associated with the Pollicott-Ruelle resonances. They are singular distributions that are smooth in the unstable phase-space directions but singular in the stable ones. This reflects the breaking of the time-reversal symmetry at the origin of these eigenmodes. Furthermore, their singular character can be demonstrated to imply the positive entropy production expected from nonequilibrium thermodynamics.

On the other hand, the nonequilibrium steady states are constructed by weighting each phase-space trajectory with a probability which is different for their time reversals. As a consequence, the invariant probability distribution describing the nonequilibrium steady state at the microscopic phase-space level explicitly breaks the time-reversal symmetry.

This time asymmetry has manifestations which can be directly tested in experiments. In particular, the transport coefficients can be obtained by considering the escape of trajectories from suitably chosen phase-space regions. The escape rate is the leading Pollicott-Ruelle resonance of these open systems and is related to the properties of the microscopic motion such as the Lyapunov exponents, the Kolmogorov-Sinai entropy per unit time, and the fractal dimensions characterizing the singularities of the nonequilibrium states. In this way, relationships have been established between the irreversible properties of transport and the characteristic quantities of the dynamical randomness and instability of the underlying microscopic dynamics. These escape-rate formulas are large-deviation relationships that include the fluctuation theorems as well as the formula (101) giving the entropy production in nonequilibrium steady states. These different relationships are given in Table IV which shows their similarities. In one version, they relate an irreversible property to the difference between rates characterizing the microscopic fluctuations. In another version, it is the ratio of two path properties which turns out to grow at a given irreversible rate. In each case, the counter term is the decay rate of some path probability, such as the Kolmogorov-Sinai entropy per unit time in the escape-rate formula or $H\left(\{\xi_\alpha\}\right)$ in the fluctuation theorem.

It is most remarkable that the entropy production in a nonequilibrium steady state is directly related to the time asymmetry in the dynamical randomness of nonequilibrium fluctuations. The entropy production turns out to be the difference in the amounts of temporal disorder between the backward and forward paths or histories. In nonequilibrium steady states, the temporal disorder $h^{\rm R}$ of the time reversals is larger than the temporal disorder

TABLE IV: Large-deviation dynamical relationships of nonequilibrium statistical mechanics.

| | | |
|---|---|---|
| transport coefficient | $\alpha = \lim_{\chi,V\to\infty} \left(\frac{\chi}{\pi}\right)^2 \left(\sum_{\lambda_i>0} \lambda_i - h_{\rm KS}\right)_\chi$ (95) | $\frac{P(\omega_0\omega_1\omega_2...\omega_{n-1})}{\lvert\Lambda(\omega_0\omega_1\omega_2...\omega_{n-1})\rvert^{-1}} \sim \exp\left[\alpha\left(\frac{\pi}{\chi}\right)^2 t\right]$ (88) |
| entropy production | $\frac{1}{k_{\rm B}}\frac{d_{\rm i}S}{dt} = h^{\rm R} - h$ (101) | $\frac{P(\omega_0\omega_1\omega_2...\omega_{n-1})}{P(\omega_{n-1}...\omega_2\omega_1\omega_0)} \sim \exp\left(\frac{t}{k_{\rm B}}\frac{d_{\rm i}S}{dt}\right)$ (102) |
| fluctuating currents | $\frac{1}{k_{\rm B}}\sum_\alpha A_\alpha\xi_\alpha = H\left(\{-\xi_\alpha\}\right) - H\left(\{\xi_\alpha\}\right)$ (140) | $\frac{P\left(\{J_\alpha=\xi_\alpha\}\right)}{P\left(\{J_\alpha=-\xi_\alpha\}\right)} \sim \exp\left(\frac{t}{k_{\rm B}}\sum_\alpha A_\alpha\xi_\alpha\right)$ (138) |

$h$ of the paths themselves. This is expressed by the *principle of temporal ordering*, according to which the typical paths are more ordered than their corresponding time reversals in nonequilibrium steady states. This principle is proved with nonequilibrium statistical mechanics and is a corollary of the second law of thermodynamics. Temporal ordering is possible out of equilibrium because of the increase of spatial disorder. There is thus no contradiction with Boltzmann's interpretation of the second law. Contrary to Boltzmann's interpretation which deals with disorder in space at a fixed time, the principle of temporal ordering is concerned by order or disorder along the time axis, in the sequence of pictures of the nonequilibrium process filmed as a movie. The emphasis of the dynamical aspects is a recent trend that finds its roots in Shannon's information theory and modern dynamical systems theory. This can explain why we had to wait the last decade before these dynamical aspects of the second law were discovered.

We here have a principle showing that the second law of thermodynamics plays a constructive role in nonequilibrium systems and thus does not have the need to exceed some threshold in the nonequilibrium constraints as was the case for the Glansdorff-Prigogine dissipative structures [67]. The principle of temporal ordering is valid as soon as the system is out of equilibrium and holds arbitrarily far from equilibrium.

These results have significant consequences in the nanosciences and biology. In nanosciences, the fluctuation theorem as well as the nonequilibrium work theorem provide a framework to understand how the nanoscale fluctuations can be taken into account, and they have recently contributed to determine thermodynamic quantities of such nanosystems as single biomolecules [68, 69]. Furthermore, these new relationships are valid arbitrarily far from equilibrium and are not limited to the linear regime. This goes along with the observation that the molecular motors typically work in the nonlinear regime [66]. Here, it should be pointed out that applications in nanosciences often deal with nonequilibrium nanosystems. In this regard, the aforementioned results are decisive contributions to the statistical thermodynamics of nonequilibrium nanosystems. The nanosciences are deeply changing the traditional view according to which the world of atoms and molecules is separated by Avogadro's number from the macroscopic world. On the one hand, it should be noticed that Avogadro's number is an artifact of the metric system conventions, and recent work shows that the macroscopic properties of thermodynamics or chemical kinetics already hold with a few hundred or thousand atoms or molecules – that is, on the scale of nanometers. Collective effects such as nonequilibrium oscillations can already emerge on this small scale [70]. On the other hand, the traditional view cannot explain why the biological systems have a multiscale architecture with molecules assembling into supramolecular structures forming organels, cells, multicellular organisms, and so on. Today, the nanosciences are discovering the existence of structures on the nanoscale in both the inorganic and organic worlds, which clearly shows that structures can exist on all scales by the interaction of atoms and molecules, contrary to the traditional view.

The biological systems are characterized by two main properties: their metabolism and their capacity to self-reproduce. The first property refers to nonequilibrium thermodynamics. Until recently, this connection between biology and thermodynamics have been limited to the macroscopic aspects. The new advances here reported open new avenues toward nonequilibrium nanosystems of biological significance such as pulled biomolecules and molecular motors. Thanks to these new advances, the thermodynamics of biological systems can nowadays apply down to the nanoscale and make the connection with molecular biology. In this perspective, the aforementioned principle of temporal ordering shows at a fundamental level how a spontaneous generation of information is possible out of equilibrium and how random fluctuations can be converted into information [71]. This question remains a puzzle from the viewpoint of equilibrium statistical mechanics because of the balance between the forward and backward

fluctuations. However, in nonequilibrium systems, the principle of temporal ordering shows that the random fluctuations should be biased, allowing the emergence of dynamical order. If this dynamical order can be memorized by the system, for instance during a process of copolymerization, we could understand that information can be generated. If furthermore this information can be restored back to the nonequilibrium dynamics of the system, the self-reproduction of biological systems could be explained. From the viewpoint given by the principle of out-of-equilibrium temporal ordering, the biological systems would be physico-chemical systems with a built-in thermodynamic arrow of time. In this sense, the principle of temporal ordering could provide an explanation of Monod's teleonomy [72] on the basis of nonequilibrium statistical mechanics and the second law of thermodynamics. In this regard, the new advances contribute to understand the origins of biological systems in the physico-chemical laws.

### Acknowledgments

The author thanks Professor G. Nicolis for support and encouragement in this research. This research was financially supported by the "Communauté française de Belgique" (contract "Actions de Recherche Concertées" No. 04/09-312).

[1] P. Gaspard, *Chaos, scattering, and statistical mechanics* (Cambridge University Press, Cambridge UK, 1998).
[2] P. Gaspard, New. J. Phys. **7**, 77 (2005).
[3] P. Gaspard, J. Stat. Phys. **117**, 599 (2004).
[4] R. Balescu, *Equilibrium and Nonequilibrium Statistical Mechanics* (Wiley, New York, 1975).
[5] G. Nicolis and I. Prigogine, *Self-Organization in Nonequilibrium Systems* (Wiley, New York, 1977).
[6] T. De Donder and P. Van Rysselberghe, *Affinity* (Stanford University Press, Menlo Park CA, 1936).
[7] L. Onsager, Phys. Rev. **37**, 405 (1931).
[8] T. Gilbert, J. R. Dorfman, and P. Gaspard, Phys. Rev. Lett. **85**, 1606 (2000).
[9] J. R. Dorfman, P. Gaspard, and T. Gilbert, Phys. Rev. E **66**, 026110 (2002).
[10] J. W. Gibbs, *Elementary Principles in Statistical Mechanics* Yale University Press, New Haven, (1902); reprinted by Dover Publ. Co., New York, (1960).
[11] C. Shannon, Bell System Tech. J. **27**, 379, 623 (1948).
[12] A. N. Kolmogorov, Dokl. Akad. Nauk SSSR **124**, 754 (1959).
[13] Ya. G. Sinai, Dokl. Akad. Nauk SSSR **124**, 768 (1959).
[14] J.-P. Eckmann and D. Ruelle, Rev. Mod. Phys. **57**, 617 (1985).
[15] E. Lorenz, J. Atmos. Sci. **20**, 130 (1963).
[16] Ya. B. Pesin, Russian Math. Surveys **32**, 55 (1977).
[17] Ch. Dellago, H. A. Posch, and W. G. Hoover, Phys. Rev. E **53**, 1485 (1996).
[18] H. van Beijeren, J. R. Dorfman, H. A. Posch, and Ch. Dellago, Phys. Rev. E **56**, 5272 (1997).
[19] P. Gaspard and H. van Beijeren, J. Stat. Phys. **109**, 671 (2002).
[20] M. Pollicott, Invent. Math. **81**, 413 (1985); Invent. Math. **85**, 147 (1986).
[21] D. Ruelle, Phys. Rev. Lett. **56**, 405 (1986); J. Stat. Phys. **44**, 281 (1986).
[22] P. Cvitanović and B. Eckhardt, J. Phys. A: Math. Gen. **24**, L237 (1991).
[23] P. Gaspard, I. Claus, T. Gilbert, and J. R. Dorfman, Phys. Rev. Lett. **86**, 1506 (2001).
[24] L. Van Hove, Phys. Rev. **95**, 249 (1954).
[25] M. S. Green, J. Chem. Phys. **20** 1281 (1952); **22**, 398 (1954).
[26] R. Kubo, J. Phys. Soc. Jpn. **12** 570 (1957).
[27] P. Gaspard, J. Stat. Phys. **68**, 673 (1992).
[28] S. Tasaki and P. Gaspard, J. Stat. Phys. **81**, 935 (1995).
[29] S. Tasaki and P. Gaspard, Bussei Kenkyu Cond. Matt. **66**, 23 (1996).
[30] T. Gilbert, J. R. Dorfman, and P. Gaspard, Nonlinearity **14**, 339 (2001).
[31] L. A. Bunimovich, and Ya. G. Sinai, Commun. Math. Phys. **78**, 247, 479 (1980).
[32] A. Knauf, Commun. Math. Phys. **110**, 89 (1987); Ann. Phys. (N. Y.) **191**, 205 (1989).
[33] I. Claus and P. Gaspard, J. Stat. Phys. **101**, 161 (2000).
[34] I. Claus and P. Gaspard, Phys. Rev. E **63**, 036227 (2001).
[35] P. Gaspard and I. Claus, Phil. Trans. Roy. Soc. Lond. A **360**, 303 (2002).
[36] I. Claus and P. Gaspard, Physica D **168-169**, 266 (2002).
[37] P. Gaspard and G. Nicolis, Phys. Rev. Lett. **65**, 1693 (1990) .
[38] P. Gaspard and F. Baras, Phys. Rev. E **51**, 5332 (1995).
[39] J. R. Dorfman and P. Gaspard, Phys. Rev. E **51**, 28 (1995).
[40] P. Gaspard and J. R. Dorfman, Phys. Rev. E **52**, 3525 (1995).
[41] E. Helfand, Phys. Rev. **119**, 1 (1960).
[42] H. van Beijeren, A. Latz, and J. R. Dorfman, Phys. Rev. E **63**, 016312 (2000).

[43] S. Viscardy and P. Gaspard, Phys. Rev. E **68**, 041204 (2003) .
[44] S. Viscardy and P. Gaspard, Phys. Rev. E **68**, 041205 (2003) .
[45] P. Gaspard and X.-J. Wang, Phys. Rep. **235**, 291 (1993).
[46] J. Schnakenberg, Rev. Mod. Phys. **48**, 571 (1976).
[47] Luo Jiu-li, C. Van den Broeck, and G. Nicolis, Z. Phys. B - Condensed Matter **56**, 165 (1984).
[48] D. J. Evans and G. P. Morriss, *Statistical Mechanics of Nonequilibrium Liquids* (Academic press, London, 1990).
[49] L. Andrey, Phys. Lett. A **11**, 45 (1985).
[50] R. Landauer, IBM J. Res. Dev. **5**, 183 (1961).
[51] C. H. Bennett, Int. J. Theor. Phys. **21**, 905 (1982).
[52] D. J. Evans, E. G. D. Cohen, and G. P. Morriss, Phys. Rev. Lett. **71**, 2401 (1993).
[53] D. J. Evans and D. J. Searles, Phys. Rev. E **50**, 1645 (1994).
[54] G. Gallavotti and E. G. D. Cohen, Phys. Rev. Lett. **74**, 2694 (1995).
[55] J. Kurchan, J. Phys. A: Math. Gen. **31**, 3719 (1998).
[56] G. E. Crooks, Phys. Rev. E **60**, 2721 (1999).
[57] J. L. Lebowitz and H. Spohn, J. Stat. Phys. **95**, 333 (1999).
[58] C. Maes, J. Stat. Phys. **95**, 367 (1999).
[59] U. Seifert, Europhys. Lett. **70**, 36 (2005).
[60] P. Gaspard, Physica A **369**, 201 (2006).
[61] C. Jarzynski, Phys. Rev. Lett. **78**, 2690 (1997).
[62] P. Gaspard, J. Chem. Phys. **120**, 8898 (2004).
[63] D. Andrieux and P. Gaspard, J. Chem. Phys. **121**, 6167 (2004).
[64] D. Andrieux and P. Gaspard, preprint cont-mat/0512254 (2005).
[65] D. Andrieux and P. Gaspard, J. Stat. Mech.: Th. Exp. P01011 (2006).
[66] D. Andrieux and P. Gaspard, Phys. Rev. E **74**, 011906 (2006).
[67] P. Glansdorff and I. Prigogine, *Thermodynamics of Structure, Stability, and Fluctuations* (Wiley-Interscience, New York, 1971).
[68] C. Bustamante, J. Liphardt, and F. Ritort, Phys. Today **58**, 43 (2005).
[69] D. Collin, F. Ritort, C. Jarzynski, S. B. Smith, I. Tinoco Jr., and C. Bustamante, Nature **437**, 231 (2005).
[70] P. Gaspard, J. Chem. Phys. **117**, 8905 (2002).
[71] M. Eigen, *Steps towards Life: A Perspective on Evolution* (Oxford University Press, Oxford, 1992).
[72] J. Monod, *Chance and Necessity* (Knopf, New York, 1971).